

Planning under Uncertainty to Goal Distributions

Adam Conkey¹ and Tucker Hermans^{1,2}

Abstract—Goals for planning problems are typically conceived of as subsets of the state space. However, for many practical planning problems in robotics, we expect the robot to predict goals, e.g. from noisy sensors or by generalizing learned models to novel contexts. In these cases, sets with uncertainty naturally extend to probability distributions. While a few works have used probability distributions as goals for planning, surprisingly no systematic treatment of planning to goal distributions exists in the literature. This article serves to fill that gap. We argue that goal distributions are a more appropriate goal representation than deterministic sets for many robotics applications. We present a novel approach to planning under uncertainty to goal distributions, which we use to highlight several advantages of the goal distribution formulation. We build on previous results in the literature by formally framing our approach as an instance of planning as inference. We additionally derive reductions of several common planning objectives as special cases of our probabilistic planning framework. Our experiments demonstrate the flexibility of probability distributions as a goal representation on a variety of problems including planar navigation among obstacles, intercepting a moving target, and a 7-DOF robot arm reaching to grasp an object. We additionally demonstrate the applicability of goal distributions in the domain of manipulation skill planning.

I. INTRODUCTION

Goals enable a robot to act with intention in its environment and provide an interface for humans to specify the desired behavior of the robot. Defining and representing goals is therefore a fundamental step in formalizing robotics problems [52, 86]. Goals are most commonly represented as elements of a (possibly infinite) subset $\mathcal{G} \subseteq \mathcal{X}$ of the robot’s state space \mathcal{X} . In practice, it is common to select a particular goal state $g \in \mathcal{G}$ to pursue, or to simply define the goal set as the singleton $\mathcal{G} = \{g\}$.

The goal state g is typically incorporated into a goal-parameterized cost function $C_g : \mathcal{X} \rightarrow \mathbb{R}$ over the robot’s state space \mathcal{X} . For example, C_g may be defined as a goal-parameterized distance function $d_g : \mathcal{X} \rightarrow \mathbb{R}$ (e.g. Euclidean distance) between the goal state g and the current state $x_t \in \mathcal{X}$. The cost function C_g is often used to monitor progress to a point-based goal [6], bias graph creation in sampling-based motion planners [52], or used directly as an objective for trajectory optimization [50]. In the latter case, an action cost is often further incorporated so that $C_g : \mathcal{X} \times \mathcal{U} \rightarrow \mathbb{R}$ can encode, for example, distance to goal while enforcing smoothness constraints on the actions $u_t \in \mathcal{U}$ from the robot’s action space \mathcal{U} .

The point-based goal formulation just described provides formal elegance but overlooks many common challenges of

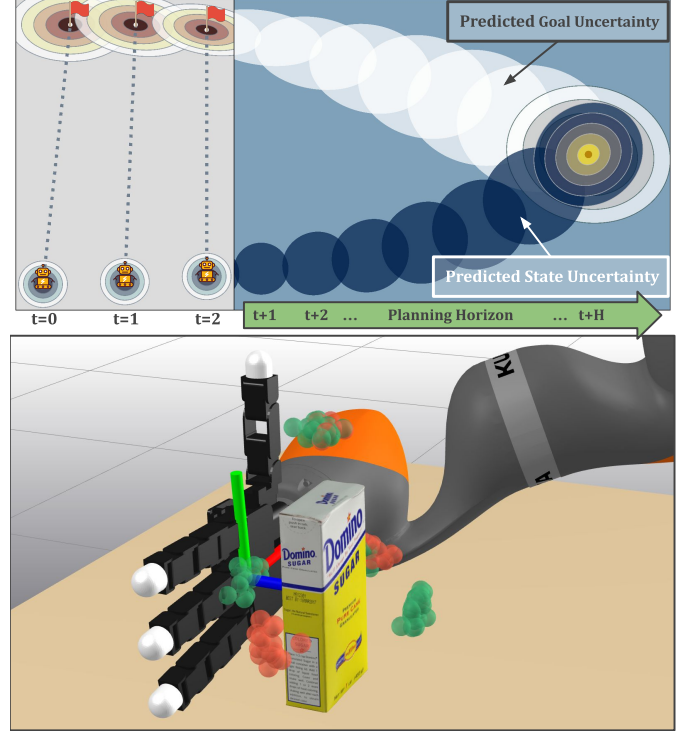


Fig. 1: Examples of goals with associated models of uncertainty. **(Upper Row)** A robot navigates to intercept a moving target (red flag) while updating a Gaussian belief about the target’s location as it acquires new observations (timesteps $t = 0$ to $t = 2$ in gray region). The robot predicts both the future goal uncertainty (white ellipses) and its own state uncertainty (blue ellipses) over the planning horizon (light blue region) to plan a path that will intercept the target (associated experiments in Sec. VIII-C).

(Lower Row) A robot arm reaches to grasp an object while inferring a reachable target pose. The goal distribution is modeled as a pose mixture model where some samples are reachable (green spheres) and others are unreachable (red spheres) based on the kinematics of the arm (associated experiments in Sec. VIII-D).

robotic systems, including stochastic dynamics, numerical imprecision, continuous state and action spaces, and uncertainty in the robot’s current state and goal. Each of these phenomena make it difficult for a robot to arrive in a desired state in a verifiable manner. As a result, it is common to utilize a catch-all fuzzy notion of goal achievement: the robot achieves its goal g if it arrives in a terminal state $x_T \in \mathcal{X}$ such that $d_g(x_T) < \varepsilon$ where $\varepsilon \in \mathbb{R}^+$ is a small tolerance governing how much error is permissible. This common relaxation fails to differentiate the various sources of uncertainty and imprecision a robot faces in pursuing a goal.

We advocate for probability distributions as a more suitable goal representation. Goals as probability distributions extend the traditional notion of set-based goals to include a measure

¹ University of Utah Robotics Center and School of Computing, University of Utah, Salt Lake City, UT, USA.

² NVIDIA Corporation, USA

Email: adam.conkey@utah.edu, thermans@cs.utah.edu

of belief (i.e. uncertainty) that a point in the state space satisfies the goal condition. Goal uncertainty arises frequently in robotics applications whenever the robot must predict its goal, e.g. estimating a goal from noisy sensors [48], forecasting a dynamic goal [43, 61], or in generalizing a learned goal representation [3, 18, 46, 70]. See Fig. 1 for a couple of examples we examine experimentally in this article. Goal distributions are also a natural representation in many domains, e.g. mixture models represent targets for distributed multi-agent systems [25, 81] and encode heuristic targets for grasping objects [18, 57, 63]. Goal distributions formally subsume traditional point-based and set-based goals as Dirac-delta and uniform distributions, respectively. In spite of the myriad use cases and benefits of goal distributions in various domains, planning and reinforcement learning frameworks continue to primarily rely on point-based goal representations, and no formal treatment of planning to goal distributions exists.

To address this gap, we formalize the use of probability distributions as a goal representation for planning (Sec. III) and discuss encoding common goal representations as distributions (Sec. IV). As our main theoretical contribution in this article, we derive a framework (Sec. V) for planning to goal distributions under state uncertainty as an instance of *planning as inference* [54, 78, 90]. Planning as inference seeks to infer an optimal sequence of actions by conditioning on achieving optimality and inferring the posterior distribution of optimal trajectories. We derive a planning as inference objective that enables the robot to plan under state uncertainty to a goal state distribution by minimizing an information-theoretic loss between its predicted state distribution and the goal distribution. We show that several common planning objectives are special cases of our probabilistic planning framework with particular choices of goal distributions and loss function (Sec. VI). We provide a practical and novel algorithm (Sec. VII) that utilizes the *unscented transform* [91] for state uncertainty propagation to efficiently compute the robot’s terminal state distribution and expected running cost.

We apply our approach to a variety of different problems, goal distributions, and planning objectives (Sec. VIII). We showcase the flexibility of probability distributions as a goal representation on the problem of planar navigation among obstacles (Sec. VIII-A). These results also exhibit the ease with which our planning framework accommodates different models of goal uncertainty simply by swapping in different goal distributions and information-theoretic losses. We provide an example of how our planning approach can leverage sources of uncertainty in the environment to achieve a target state distribution (Sec. VIII-B) in a ball-rolling task. We also apply our approach to the problem of intercepting a moving target in which the agent updates its belief of the goal as it acquires noisy observations of the target (Sec. VIII-C). We investigate a higher-dimensional problem in which a 7-DOF robot arm reaches to grasp an object (Sec. VIII-D), where we model target end-effector poses as a mixture of pose distributions about the object. We show that we are able to plan to reachable poses using this distribution directly as our goal representation without checking for reachability, while a point-based goal requires computing inverse kinematics to check

reachability prior to planning. Finally, we apply our approach to the more challenging domain of manipulation skill planning (Sec. VIII-E), which requires learning a dynamics model to support planning over the contact dynamics involved in dynamic manipulations. We show we are able to accommodate more dynamic skills than are typically used in skill planning while also explicitly representing the uncertainty inherent to common manipulation goals.

We conclude the article in Sec. IX, where we discuss the opportunities to expand the use of goal distributions in other existing planning as inference frameworks (e.g. reinforcement and imitation learning).

II. RELATED WORK

We first review works on planning as inference, since we formally situate the problem of planning to goal distributions as an instance of planning as inference. Planning as inference has proven to be a powerful framework to formalize problems in robotics [5, 50, 54, 64, 78, 90, 95]. It constitutes a Bayesian view of stochastic optimal control [50, 78, 90] from which popular decision-making algorithms can be derived such as max-entropy reinforcement learning [54] and sampling-based solvers like model-predictive path integral control (MPPI) [9, 50, 96] and the cross-entropy method (CEM) [44, 50]. The probabilistic perspective of planning as inference enables elegant problem definitions as factor graphs that can be solved by message-passing algorithms [90, 95] and non-linear least squares optimizers [64]. Goal distributions have not been explicitly considered in the planning as inference framework. Part of our contribution in this article is formulating the problem of planning to goal distributions as an instance of planning as inference, thereby connecting to the rich literature on planning as inference and enabling access to a variety of existing algorithms to solve the problem.

As mentioned in Sec. I, goal distributions have cropped up in various sub-domains of robotics, but the topic has not yet received systematic attention. The closest work we are aware of is [67] which advocates for goal-distribution-conditioned policies as an extension to goal-conditioned policies in reinforcement learning. A limited class of goal distributions are considered in [67] and the formulation is specific to reinforcement learning. We view the present article as complementary to [67], where we consider more general classes of goal distributions and develop an approach for planning to goal distributions in a unified way.

Target distributions have been utilized in reinforcement learning to encourage exploration [53] and expedite policy learning [4]. *State marginal matching* [53] learns policies for which the state marginal distribution matches a target distribution (typically uniform) to encourage targeted exploration of the environment. Goal distributions have also been used as sample generators for goal-conditioned reinforcement learning [66, 76]. Recent improvements on *hindsight experience replay* (HER) [4] have sought to estimate goal distributions that generate samples from low density areas of the replay buffer state distribution [47, 74, 101] or that form a curriculum of achievable goals [79, 74]. We note that HER-based methods

are typically used in multi-goal reinforcement learning where states are interpreted as goals irrespective of their semantic significance as a task goal.

A closely related but distinct area of research is *covariance steering* [36] which optimizes feedback controller parameters and an open-loop control sequence to move a Gaussian state distribution to a target Gaussian distribution. Recent work on covariance steering has focused on satisfying chance constraints [68, 73, 80], including generating constraint-satisfying samples for MPPI [99]. Covariance steering typically assumes linear dynamics and is limited to Gaussian state distributions, where the objective is often to ensure the terminal state covariance is fully contained within the goal state covariance. Covariance steering also decouples control of the distribution into *mean steering* and *covariance steering*, which assumes homogeneous uncertainty and accuracy of control over the state space. These assumptions do not hold for most robotics domains. For example, visual odometry estimates degrade when entering a dark room [89], and it is harder to maneuver over varied terrain [21]. In contrast, our approach easily accommodates non-linear dynamics, non-homogeneous state uncertainty, and non-Gaussian state distributions.

We utilize information-theoretic costs in our approach as they are fitting objectives for optimizing plans to goal distributions. A variety of information theoretic costs have been utilized in planning and policy optimization which we briefly review here. Probabilistic control design [49] minimizes Kullback-Leibler (KL) divergence between controlled and desired state-action distributions and bears some similarity to planning as inference previously described. KL divergence is also commonly used to constrain optimization iterations in policy search [16, 72, 82] and planning [2]. Broader classes of divergences including f -divergence [8, 28, 41] and Tsallis divergence [94] have also been utilized for policy improvement [8], imitation learning [28, 41], and stochastic optimal control [94]. Stochastic optimal control and planning techniques often seek to minimize the expected cost of the trajectory [23, 97] or maximize the probability of reaching a goal set [13, 55]. Entropy of a stochastic policy is utilized in maximum-entropy reinforcement learning [33, 34, 2] and inverse reinforcement learning [103] to prevent unnecessarily biasing the policy class. We demonstrate the use of cross-entropy and KL divergence in our formulation of planning to goal distributions. However, our approach is general enough to admit other information-theoretic losses between the robot's predicted state distribution and a goal distribution. We discuss this point further in Sec. IX.

III. PROBLEM STATEMENT

We focus our work on planning problems with continuous state and action spaces in which the robot must reach a desired goal while acting under stochastic dynamics. These problems fall in the domain of stochastic optimal control and planning [85, 78]. We consider a robot with continuous state space $\mathcal{X} \subseteq \mathbb{R}^{N_x}$ and continuous action space $\mathcal{U} \subseteq \mathbb{R}^{N_u}$ and focus on a discrete time setting, although extending to continuous time would be straightforward. The stochastic

dynamics function $f : \mathcal{X} \times \mathcal{U} \times \Omega \rightarrow \mathcal{X}$ determines the resulting state $\mathbf{x}_{t+1} = f(\mathbf{x}_t, \mathbf{u}_t, \boldsymbol{\omega}_t)$ from applying action $\mathbf{u}_t \in \mathcal{U}$ in state $\mathbf{x}_t \in \mathcal{X}$ at time t subject to noise $\boldsymbol{\omega}_t \sim \Omega$.

Planning to a goal state $\mathbf{g} \in \mathcal{X}$ in this setting requires the agent to utilize the dynamics function f to find a sequence of actions $\mathbf{u}_0, \dots, \mathbf{u}_{T-1} \in \mathcal{U}^T$ from its initial state¹ $\mathbf{x}_0 \in \mathcal{X}$ to the goal state \mathbf{g} . Due to sensor noise and partial observability, the robot rarely knows its current state precisely and must therefore plan from an initial estimated distribution of states $\hat{p}(\mathbf{x}_0)$, e.g. as the output of a state estimator like a Kalman filter [89]. Typically the robot must minimize the expected cost under state uncertainty and stochastic dynamics defined by a cost function $C : \mathcal{X} \times \mathcal{U} \rightarrow \mathbb{R}$. As noted in Sec. I, the cost function typically includes a distance function parameterized by \mathbf{g} to induce goal-seeking behavior.

Instead of planning to particular states, we consider the more general problem of planning to a *goal state distribution*. A goal distribution $p(\mathbf{x}|\mathbf{g} = 1)$ encodes the robot's belief (i.e. uncertainty) that a particular state \mathbf{x} belongs to the goal set \mathcal{G} . Using Bayes rule, we see for any particular \mathbf{x} the goal density is proportional to the goal likelihood $p(\mathbf{x}|\mathbf{g} = 1) \propto p(\mathbf{g} = 1|\mathbf{x})$. We abbreviate the goal distribution as $p_{\mathbf{g}}(\mathbf{x})$. In this article, we assume the goal distribution is given in order to focus our efforts on formalizing the problem of planning to goal distributions. We note that goal distributions can be set as desired if known in parametric form, which can be as simple as adding uncertainty bounds to a point-based goal, e.g. adding a Gaussian covariance or setting uniform bounds on a region centered about a target point. Goal distributions can also be estimated from data [3, 18, 46, 70]. We discuss this point further in Sec. IX.

Given a goal distribution, we require two main ingredients to generate a plan to it. First, we need a means of predicting the robot's terminal state distribution after following a planned sequence of actions. This is a form of state uncertainty propagation which we discuss further in Sec. VII-A. Second, we require a loss function $\mathcal{L} : \mathcal{Q} \times \mathcal{P} \rightarrow \mathbb{R}$ that quantifies the difference between distributions $q \in \mathcal{Q}$ and $p \in \mathcal{P}$, where \mathcal{Q} and \mathcal{P} are arbitrary families of distributions. In particular, we are interested in quantifying the difference between the robot's terminal state distribution and the goal state distribution. Typically \mathcal{L} will take the form of a statistical divergence (e.g. KL divergence, total variation, etc.), but we leave open the possibility for other losses which may not meet the formal definition of a divergence (e.g. cross-entropy).

We can now formally state our problem as minimizing the information-theoretic loss \mathcal{L} between the terminal state distribution $q(\mathbf{x}_T | \mathbf{X}_{T-1}, \mathbf{U}_{T-1})$ and $p_{\mathbf{g}}(\mathbf{x}_T)$, where we abbreviate $\mathbf{U}_t \doteq (\mathbf{u}_0, \dots, \mathbf{u}_t)$, and $\mathbf{X}_t \doteq (\mathbf{x}_0, \dots, \mathbf{x}_t)$. We formulate this as the following constrained optimization

¹We use \mathbf{x}_0 to indicate the state from which the agent is planning, but note the timestep is arbitrary and replanning from any timestep is permissible, as is common in model-predictive control schemes [50, 96].

problem

$$\operatorname{argmin}_{\pi} \mathcal{L}(q(\mathbf{x}_T | \mathbf{X}_{T-1}, \mathbf{U}_{T-1}), p_g(\mathbf{x}_T)) \quad (1a)$$

$$+ \mathbb{E}_{q(\mathbf{X}_{T-1}, \mathbf{U}_{T-1})} \left[\sum_{t=0}^{T-1} c_t(\mathbf{x}_t, \mathbf{u}_t) \right] \quad (1b)$$

$$\text{s.t.} \quad \mathbf{X}_T \in \mathcal{X}^T, \mathbf{U}_{T-1} \in \mathcal{U}^T \quad (1c)$$

$$q(\mathbf{x}_0) = \hat{p}(\mathbf{x}_0) \quad (1d)$$

where π defines the policy being optimized. In its simplest form, the policy can just be a sequence of actions $\pi = \mathbf{U}_{T-1}$, but we note that more general policy parameterizations can also be utilized. The sequence of states \mathbf{X}_t is induced by the dynamics function f together with the sequence of actions \mathbf{U}_t . Eq. 1a is the loss between the terminal state distribution under the policy and the goal distribution. Eq. 1b is the expected cost accumulated over the trajectory, where $c_t : \mathcal{X} \times \mathcal{U} \rightarrow \mathbb{R}$ encapsulates arbitrary running costs. Eq. 1c ensures states and actions are from the robot's state-action space. Eq. 1d is a constraint that ensures planning initiates from the robot's belief about its initial state.

We present a more concrete instantiation of this optimization problem in Sec. VII-A where we present a tractable method for computing the terminal state distribution utilized in the information-theoretic loss in Eq. 1a. Before diving into the details of our planning formulation in Sec. V, we first define some useful goal distributions in Sec. IV.

IV. GOAL DISTRIBUTIONS

We present a selection of goal distributions we explore in this article. Our list is by no means exhaustive and we emphasize there are likely domains that benefit from less standard distributions [1].

A. Dirac-delta

A Dirac-delta distribution has a density function with infinite density at its origin point \mathbf{p} and zero at all other points:

$$\delta_{\mathbf{p}}(\mathbf{x}) = \begin{cases} \infty & \text{if } \mathbf{x} = \mathbf{p} \\ 0 & \text{otherwise} \end{cases} \quad (2)$$

such that $\int_{\mathcal{X}} \delta_{\mathbf{p}}(\mathbf{x}) d\mathbf{x} = 1$ over its domain \mathcal{X} . The Dirac-delta is a probabilistic representation of a point-based goal [15]. Point-based goals are the most common goal representation in both planning [52] and reinforcement learning [86].

B. Uniform

A uniform distribution is a probabilistic representation of a set-based goal and has the density function

$$\mathbb{U}_A(\mathbf{x}) = \begin{cases} \frac{1}{\text{vol}(A)} & \text{if } \mathbf{x} \in A \\ 0 & \text{otherwise} \end{cases} \quad (3)$$

where $\text{vol}(A)$ defines the volume of the set A . Uniform distributions are useful for encoding a bounded region of acceptable goal states without any preference to any particular state within that region. Examples include navigating to be in a particular room [98], or placing an object on a desired region

of a table surface [20]. Uniform goal distributions have also proven useful as goal sample generators, particularly when learned to bias goal-conditioned policies to reach desirable states [76].

C. Gaussian

A Gaussian distribution has the density function

$$\mathcal{N}(\mathbf{x} | \boldsymbol{\mu}, \boldsymbol{\Sigma}) = \frac{1}{\sqrt{(2\pi)^d |\boldsymbol{\Sigma}|}} \exp\left(-\frac{1}{2} d_M(\mathbf{x}; \boldsymbol{\mu}, \boldsymbol{\Sigma})^2\right) \quad (4)$$

where $\boldsymbol{\mu}$ and $\boldsymbol{\Sigma}$ define the mean and covariance of the distribution, respectively, and $d_M(\mathbf{x}; \boldsymbol{\mu}, \boldsymbol{\Sigma}) = \sqrt{(\mathbf{x} - \boldsymbol{\mu})^T \boldsymbol{\Sigma}^{-1} (\mathbf{x} - \boldsymbol{\mu})}$ is the *Mahalanobis distance* [62]. Gaussian distributions have been utilized in learning from demonstration to encode goals learned in a data-driven fashion from sub-optimal experts [3, 18, 46, 70]. Gaussians also naturally encode uncertainty the agent might have about its goal, e.g. in dynamic tasks like object handovers [61] and catching moving objects [43], or estimating a goal online from noisy observations, e.g. footstep planning [48].

We also consider a truncated Gaussian [87] distribution with density function

$$\mathcal{N}(\mathbf{x} | \boldsymbol{\mu}, \boldsymbol{\Sigma}, \mathcal{A}) = \begin{cases} \frac{\exp(-\frac{1}{2} d_M(\mathbf{x}; \boldsymbol{\mu}, \boldsymbol{\Sigma})^2)}{\int_{\mathcal{A}} \exp(-\frac{1}{2} d_M(\mathbf{x}; \boldsymbol{\mu}, \boldsymbol{\Sigma})^2) d\mathbf{x}} & \text{if } \mathbf{x} \in \mathcal{A} \\ 0 & \text{otherwise} \end{cases} \quad (5)$$

which is a common model for bounded Gaussian uncertainty [19].

D. Bingham

The Bingham distribution [11] is an antipodally symmetric distribution on the unit hypersphere \mathbb{S}^d with density function

$$\mathcal{B}(\mathbf{x} | \Lambda, V) = \frac{1}{F(\Lambda)} \exp\left(\sum_{i=1}^d \lambda_i (\mathbf{v}_i^T \mathbf{x})^2\right) \quad (6)$$

where $\mathbf{x} \in \mathbb{S}^d \subset \mathbb{R}^{d+1}$ is constrained to the unit hypersphere \mathbb{S}^d , Λ is a diagonal matrix of concentration parameters, the columns of V are orthogonal unit vectors, and $F(\Lambda)$ is a normalization constant. The Bingham density function bears resemblance to the multivariate Gaussian density function because it is derived from a zero-mean Gaussian conditioned to lie on the unit hypersphere \mathbb{S}^d .

The Bingham distribution on \mathbb{S}^3 is of particular interest to robotics as it encodes a Gaussian distribution over orientations in 3D [31]. The key difficulty in utilizing the Bingham distribution is computing the normalization constant $F(\Lambda)$ since no closed-form solution exists. In spite of this, efficient and accurate approximations have enabled use of the Bingham distributions for 6-DOF object pose estimation [32], tracking of moving objects [31], and pose uncertainty quantification in deep neural networks [71].

E. Mixture Models

Mixture models comprise a weighted combination of multiple probability distributions. A Gaussian mixture model (GMM) is the most commonly used mixture model with density function

$$\mathcal{M}(\mathbf{x} \mid \{\alpha_i, \boldsymbol{\mu}_i, \boldsymbol{\Sigma}_i\}_{i=1}^M) = \sum_{i=1}^M \alpha_i \mathcal{N}(\mathbf{x} \mid \boldsymbol{\mu}_i, \boldsymbol{\Sigma}_i) \quad (7)$$

where $\{\alpha_i\}_{i=1}^M$ are mixture weights associated with each component such that $\sum_{i=1}^M \alpha_i = 1$. GMMs have been used to encode goals learned in a data-driven fashion where a single mode does not suffice, such as the desired pre-grasp pose to pick up an object [18, 57, 63]. Mixture models also provide a natural goal representation for distributed multi-agent systems [25, 81]. We highlight that mixture models are not limited to mixtures of Gaussians and that other distribution families are possible. For example, a mixture of uniform distributions probabilistically encodes a union of disjoint goal sets [10].

F. Goal Likelihood Classifier

We can model the likelihood that a state achieves goal $p(\mathbf{g} = 1 \mid \mathbf{x}) = f(\mathbf{x}; \theta)$ using a discriminative classifier, such as logistic regression, parameterized by θ . This model offers great flexibility [26] and can be used to model complex goal relations such as planning to achieve grasps for multi-fingered hands [58] and deformable object manipulation from image observations [84].

V. PLANNING TO GOAL DISTRIBUTIONS

Our proposed use of goal distributions discussed in Sec. III fits naturally within the methods of *planning and control as probabilistic inference* [54, 78]. In this section, we first present a background on traditional planning as inference frameworks in Sec V-A. We then provide our novel derivation and theoretical analysis of planning to goal distributions within the planning as inference framework Sec. V-B.

A. Planning as Inference

Planning as inference leverages a duality between optimization and probabilistic inference for motion control and planning problems [54, 78, 90]. In the planning as inference framework, we consider distributions of state-action trajectories $p(\tau)$ where $\tau = (\mathbf{X}_T, \mathbf{U}_{T-1})$. We introduce a binary random variable $\mathcal{O}_\tau \in \{0, 1\}$ where values of $\mathcal{O}_\tau = 1$ and $\mathcal{O}_\tau = 0$ denote whether a trajectory τ is optimal or not, respectively. We use the notation \mathcal{O}_τ to represent $\mathcal{O}_\tau = 1$ for brevity, and similarly we use \mathcal{O}_t to represent $\mathcal{O}_t = 1$ to denote optimality at a particular timestep in the trajectory τ . We treat optimality as an observed quantity and seek to infer the posterior distribution of optimal trajectories $p(\tau \mid \mathcal{O}_\tau)$. Algorithms based on variational inference are commonly used to optimize a proposal distribution $q(\tau)$ from a known family \mathcal{Q} (e.g. exponential) by solving the following minimization:

$$q^* = \operatorname{argmin}_{q \in \mathcal{Q}} \operatorname{D}_{\text{KL}}(q(\tau) \parallel p(\tau \mid \mathcal{O}_\tau)) \quad (8)$$

This minimization is equivalently solved by (details in Appendix A)

$$q^* = \operatorname{argmin}_{q \in \mathcal{Q}} \underbrace{-\mathbb{E}_q[\log p(\mathcal{O}_\tau \mid \tau)]}_{T_1} + \underbrace{\operatorname{D}_{\text{KL}}(q(\tau) \parallel p_0(\tau))}_{T_2} \quad (9)$$

where we have labeled the first and second terms in Eq. 9 as T_1 and T_2 , respectively, for ease of reference in Sec. V-B.

The objective in Eq. 9 seeks to maximize the log-likelihood of being optimal in expectation under the trajectory while being regularized by a state-action trajectory prior $p_0(\tau)$. A salient example of a trajectory prior from the literature is a Gaussian process prior to ensure trajectory smoothness [64]. The state-action trajectory distribution $p_0(\tau)$ is induced by the stochastic policy prior $\pi_0(\mathbf{u}_t \mid \mathbf{x}_t)$. We elaborate further on different prior policies in Sec. V-B.

The likelihood $p(\mathcal{O}_\tau \mid \tau)$ in Eq. 9 is key to planning as inference, as it connects the optimization to task-specific objectives. The likelihood may be set to any density function, but it is most commonly set as the exponentiated negative cost [78]:

$$p(\mathcal{O}_\tau \mid \tau) = \exp(-\alpha C(\tau)) \quad (10)$$

for $C(\tau) = c_{\text{term}}(\mathbf{x}_T) + \sum_{t=0}^{T-1} c_t(\mathbf{x}_t, \mathbf{u}_t)$ where $c_{\text{term}}(\cdot)$ is a terminal cost function defined for the final timestep in the planning horizon and $c_t(\cdot, \cdot)$ is the cost function for all other timesteps.

We have so far presented planning as inference in its standard formulation akin to [78] and [50]. We now turn to our novel contributions to incorporate goal distributions in planning as inference.

B. Goal Distributions in Planning as Inference

We examine incorporating goal distributions into the planning as inference framework just described and derive its relation to the optimization problem from Eq. 1.

We first address the optimality likelihood $p(\mathcal{O}_\tau \mid \tau)$. We define optimality at the terminal state to mean reaching the goal, i.e. $p(\mathcal{O}_T) = p_g(\mathbf{x}_T)$. We then define the trajectory optimality likelihood as

$$p(\mathcal{O}_\tau \mid \tau) = p_g(\mathbf{x}_T) \exp\left(-\alpha \sum_{t=0}^{T-1} c_t(\mathbf{x}_t, \mathbf{u}_t)\right) \quad (11)$$

which captures our proposed notion of optimality, namely satisfying high probability under the goal distribution density function $p_g(\mathbf{x}_T)$ while accounting for arbitrary running costs over the rest of the trajectory. We note this is equivalent to defining $c_{\text{term}} = -\frac{1}{\alpha} \ln p_g(\mathbf{x}_T)$ in Eq. 10. However, since $p_g(\mathbf{x}_T)$ is a density function, we find it more appropriate to directly incorporate it as a factor in the optimality likelihood.

We now consider the implications of using the optimality likelihood from Eq. 11 by plugging it into Eq. 9. Plugging

Eq. 11 into T_1 we get

$$T_1 = -\mathbb{E}_q \left[\log \left(p_g(\mathbf{x}_T) \exp \left(-\alpha \sum_{t=0}^{T-1} c_t(\mathbf{x}_t, \mathbf{u}_t) \right) \right) \right] \quad (12)$$

$$= -\mathbb{E}_q \left[\log p_g(\mathbf{x}_T) + \log \exp \left(-\alpha \sum_{t=0}^{T-1} c_t(\mathbf{x}_t, \mathbf{u}_t) \right) \right] \quad (13)$$

$$= \underbrace{\mathbb{E}_q [-\log p_g(\mathbf{x}_T)]}_{T_3} + \underbrace{\mathbb{E}_q \left[\alpha \sum_{t=0}^{T-1} c_t(\mathbf{x}_t, \mathbf{u}_t) \right]}_{T_4} \quad (14)$$

where T_4 is simply the expected running cost accumulated over non-terminal timesteps of the trajectory, which we inherit from the standard planning as inference formulation. Our formulation differs for the final timestep with term T_3 which we further expand as $T_3 = \mathbb{E}_q [-\log p_g(\mathbf{x}_T)] = \mathbb{E}_{q(\mathbf{x}_T|\tau)} [-\log p_g(\mathbf{x}_T)]$. This quantity is the *cross-entropy* of $p_g(\mathbf{x}_T)$ with respect to the terminal state distribution $q(\mathbf{x}_T | \tau)$ which we denote by $\mathcal{H}(q(\mathbf{x}_T | \tau), p_g(\mathbf{x}_T))$.

Recombining the terms above, we restate the planning as inference objective from Eq 8 for the case of planning to goal distributions as

$$q^* = \underset{q \in \mathcal{Q}}{\operatorname{argmin}} \mathcal{H}(q(\mathbf{x}_T | \tau), p_g(\mathbf{x}_T)) + \mathbb{E}_q \left[\alpha \sum_{t=0}^{T-1} c_t(\mathbf{x}_t, \mathbf{u}_t) \right] + D_{\text{KL}}(q(\tau) \parallel p_0(\tau)) \quad (15)$$

Remark 1. *Planning as inference for planning to goal distributions is equivalent to minimizing the cross-entropy between the terminal state distribution and the goal distribution while minimizing expected running costs and regularizing to a prior state-action distribution.*

We now discuss some special cases of this result and relate the objective from Eq. 15 to the optimization problem we defined in Eq. 1.

1) *Deterministic Policy:* If we assume a deterministic policy $\pi(\mathbf{u}_t | \mathbf{x}_t) = \delta_{\mathbf{u}_t = \phi(\mathbf{x}_t)}$, then the KL regularization term in Eq. 15 reduces to $D_{\text{KL}}(q(\tau) \parallel p_0(\tau)) = \mathbb{E}_q \left[-\sum_{t=0}^{T-1} \log \pi_0(\mathbf{u}_t | \mathbf{x}_t) \right]$ (see Appendix B for details) and we simplify Eq. 15 to

$$q^* = \underset{q \in \mathcal{Q}}{\operatorname{argmin}} \mathcal{H}(q(\mathbf{x}_T | \tau), p_g(\mathbf{x}_T)) + \mathbb{E}_q \left[\alpha \sum_{t=0}^{T-1} c_t(\mathbf{x}_t, \mathbf{u}_t) \right] + \mathbb{E}_q \left[-\sum_{t=0}^{T-1} \log \pi_0(\mathbf{u}_t | \mathbf{x}_t) \right] \quad (16)$$

We assume a deterministic policy in the rest of this article. We discuss extensions for reinforcement learning later in Sec. IX.

2) *Uniform Prior Policy:* If we specify a uniform distribution for the policy prior $\pi_0(\mathbf{u}_t | \mathbf{x}_t) = \mathcal{U}(\mathbf{u}_t)$, its value becomes constant with respect to the optimization [78], reducing the problem to exactly that defined in Eq. 1a with the cross entropy as loss $\mathcal{L}(q(\mathbf{x}_T | \tau), p_g(x)) = \mathcal{H}(q(\mathbf{x}_T | \tau), p_g(x))$.

Remark 2. *Planning as inference for planning to goal distributions with a uniform prior policy is equivalent to solving the planning to goal distribution problems with a cross entropy loss.*

3) *Maximum Entropy Terminal State:* We consider setting the loss in Eq. 1a to be the KL-divergence, $D_{\text{KL}}(q(\mathbf{x}_T|\tau) \parallel p_g(x))$. Then we have the following objective for the planning to goal distribution problem

$$q^* = \underset{q \in \mathcal{Q}}{\operatorname{argmin}} D_{\text{KL}}(q(\mathbf{x}_T|\tau) \parallel p_g(\mathbf{x}_T)) + \mathbb{E}_q \left[\alpha \sum_{t=0}^{T-1} c_t(\mathbf{x}_t, \mathbf{u}_t) \right] \quad (17)$$

$$= \underset{q \in \mathcal{Q}}{\operatorname{argmin}} \mathcal{H}(q(\mathbf{x}_T|\tau), p_g(\mathbf{x}_T)) + \mathbb{E}_q \left[\alpha \sum_{t=0}^{T-1} c_t(\mathbf{x}_t, \mathbf{u}_t) \right] - \mathcal{H}(q(\mathbf{x}_T|\tau)) \quad (18)$$

following from the relation $\mathcal{H}(p_1, p_2) = D_{\text{KL}}(p_1 \parallel p_2) + \mathcal{H}(p_1)$. If we set Eq. 18 equal to Eq. 16 we see the first two terms cancel and we are left with the equality

$$\mathcal{H}(q(\mathbf{x}_T|\tau)) = \mathbb{E}_q \left[\sum_{t=0}^{T-1} \log \pi_0(\mathbf{u}_t | \mathbf{x}_t) \right] \quad (19)$$

Remark 3. *Planning as inference for planning to goal distributions with a prior policy that maximizes entropy of the terminal state is equivalent to solving the planning to goal distributions problem with a KL divergence loss.*

4) *M-Projections for Planning to Finite Support Goals:* The KL divergence in the variational inference objective for planning as inference in Eq. 8 is formulated as an information projection. Since KL divergence is an asymmetric loss between distributions, there are two possible projections an optimizer can solve to minimize KL divergence:

$$q^* = \underset{q}{\operatorname{argmin}} D_{\text{KL}}(q(x) \parallel p(x)) \quad (\text{I-projection})$$

$$q^* = \underset{q}{\operatorname{argmin}} D_{\text{KL}}(p(x) \parallel q(x)) \quad (\text{M-projection})$$

The information projection (I-projection) exhibits mode-seeking behavior while the moment projection (M-projection) seeks coverage of all regions where $p(x) > 0$ and thus exhibits moment-matching behavior [65]. Importantly, when $p(x)$ has finite support (e.g. uniform, Dirac-delta, truncated Gaussian), it is necessary to use an M-projection to avoid the division by zero that would occur in the I-projection over regions outside the support of $p(x)$.

Our formulation has so far only considered an I-projection. In general, the M-projection is intractable to solve for arbitrary planning as inference problems. This is due to the fact that one would require access already to the full distribution of optimal trajectories $p(\tau | \mathcal{O}_\tau)$ in order to compute the optimization. However, since we do assume access to the goal distribution, we *can* compute either the I-projection or M-projection for the KL divergence at the terminal timestep. Thus as a final objective for investigation, we examine setting the distributional loss in Eq. 1a to be the M-projection KL

divergence, instead of the I-projection as previously examined. We get the following objective:

$$\pi^* = \underset{\pi}{\operatorname{argmin}} D_{\text{KL}} \left(p_g(\mathbf{x}_T) \parallel q(\mathbf{x}_T | \tau) \right) + \mathbb{E}_q \left[\alpha \sum_{t=0}^{T-1} c_t(\mathbf{x}_t, \mathbf{u}_t) \right] \quad (20)$$

This is nearly equivalent to the planning as inference with a maximum-entropy prior result from Sec. V-B3, however the KL divergence term is now an M-projection. A key advantage this affords us is our method naturally accommodates goal distributions with finite support, which we explore in our experiments in Sec. VIII-A. We thus have a unified framework for planning to arbitrary goal distributions under uncertain dynamics utilizing information-theoretic loss functions.

Note that for a fixed goal distribution, the M-projection of cross-entropy is equivalent to the objective in Eq. 20 since the entropy of the goal distribution is constant with respect to the decision variables. However, this is not necessarily the case for goal distributions that may change over time based on the agent's observations. We discuss this point further in Sec. IX.

VI. COST REDUCTIONS

We present an additional theoretical contribution to illustrate how our probabilistic planning framework encompasses common planning objectives in the literature. We examine the cross-entropy cost term (term T_3 in Eq. 14) between the predicted terminal state distribution $q(\mathbf{x}_T | \tau)$ and the goal distribution $p_g(\mathbf{x}_T)$ for several common distribution choices. Looking at both the I-projection $D_{\text{CE}}(q(\mathbf{x}_T | \tau) \parallel p_g(\mathbf{x}_T))$ and the M-projection $D_{\text{CE}}(p_g(\mathbf{x}_T) \parallel q(\mathbf{x}_T | \tau))$, we reduce the costs to commonly used cost functions from the literature.

A. (Weighted) Euclidean Distance

For a Gaussian goal distribution $p_g(\mathbf{x}_T) = \mathcal{N}(\mathbf{x}_T | \boldsymbol{\mu}_g, \boldsymbol{\Sigma}_g)$ and minimizing the I-projection of cross-entropy we have:

$$\pi^* = \underset{\pi}{\operatorname{argmin}} \mathbb{E}_{q(\tau)} [-\log \mathcal{N}(\mathbf{x}_T | \boldsymbol{\mu}_g, \boldsymbol{\Sigma}_g)] \quad (21)$$

$$= \underset{\pi}{\operatorname{argmin}} \mathbb{E}_{q(\tau)} [-\log \exp\{-(\mathbf{x}_T - \boldsymbol{\mu}_g)^T \boldsymbol{\Sigma}_g^{-1} (\mathbf{x}_T - \boldsymbol{\mu}_g)\}] \quad (22)$$

$$= \underset{\pi}{\operatorname{argmin}} \mathbb{E}_{q(\tau)} [(\mathbf{x}_T - \boldsymbol{\mu}_g)^T \boldsymbol{\Sigma}_g^{-1} (\mathbf{x}_T - \boldsymbol{\mu}_g)] \quad (23)$$

$$= \underset{\pi}{\operatorname{argmin}} \mathbb{E}_{q(\tau)} \left[\|\mathbf{x}_T - \boldsymbol{\mu}_g\|_{\boldsymbol{\Sigma}_g^{-1}}^2 \right] \quad (24)$$

$$= \underset{\pi}{\operatorname{argmin}} \mathbb{E}_{q(\tau)} \left[\|\mathbf{x}_T - \boldsymbol{\mu}_g\|_{\boldsymbol{\Lambda}_g}^2 \right] \quad (25)$$

For the case of deterministic dynamics, that is $q(\mathbf{x}_T | \tau) = \delta_{\mathbf{x}_T | \tau}(\mathbf{x})$, the expectation simplifies to a single point evaluation and we recover the common weighted Euclidean distance. Since it is weighted by the precision (i.e. inverse covariance) of the goal distribution, it is equivalent to the Mahalanobis distance [62]. The same cost arises for the case of a goal point (i.e. Dirac delta distribution) and Gaussian state uncertainty if we consider the M-projection of cross-entropy. In this case, the distance is weighted by the precision of the terminal state distribution instead of the goal precision.

B. Goal Set Indicator

For a uniform goal distribution $p_g(\mathbf{x}) = \mathbb{U}_{\mathcal{G}}(\mathbf{x})$ and deterministic dynamics $q(\mathbf{x}_T | \tau) = \delta_{\mathbf{x}_T | \tau}(\mathbf{x})$, minimizing the I-projection of cross-entropy amounts to

$$\pi^* = \underset{\pi}{\operatorname{argmin}} \mathbb{E}_{q(\tau)} [-\log \mathbb{U}_{\mathcal{G}}(\mathbf{x})] \quad (26)$$

$$= \underset{\pi}{\operatorname{argmin}} \int_{\mathbf{x} \in \{\mathbf{x}_T\}} -\delta_{\mathbf{x}_T | \tau}(\mathbf{x}) \log \mathbb{U}_{\mathcal{G}}(\mathbf{x}) d\mathbf{x} \quad (27)$$

$$= \underset{\pi}{\operatorname{argmin}} \begin{cases} -\log u_{\mathcal{G}} & \text{if } \mathbf{x}_T \in \mathcal{G} \\ \infty & \text{otherwise} \end{cases} \quad (28)$$

where $u_{\mathcal{G}} = 1/|\mathcal{G}|$ as described in Sec. IV-B. Hence the minimum is obtained with a constant cost if the terminal state \mathbf{x}_T from executing trajectory τ reaches any point in the goal set, while any state outside the goal set receives infinite cost. Note the function is non-differentiable as expected from the set-based goal definition. We can treat a single goal state naturally as a special case of this function. The non-differentiable nature of this purely set-based formulation motivates using search-based and sampling-based planners over optimization-based approaches in these deterministic settings.

C. Chance-Constrained Goal Set

For a uniform goal distribution $p_g(\mathbf{x}) = \mathbb{U}_{\mathcal{G}}(\mathbf{x})$, minimizing the M-projection of cross-entropy amounts to

$$\pi^* = \underset{\pi}{\operatorname{argmin}} \mathbb{E}_{\mathbb{U}_{\mathcal{G}}(\mathbf{x})} [-\log q(\mathbf{x}_T | \tau)] \quad (29)$$

$$= \underset{\pi}{\operatorname{argmin}} \int_{\mathbf{x} \in \mathcal{G}} -\mathbb{U}_{\mathcal{G}}(\mathbf{x}) \log q(\mathbf{x}_T | \tau) d\mathbf{x} \quad (30)$$

$$= \underset{\pi}{\operatorname{argmin}} -u_{\mathcal{G}} \int_{\mathbf{x} \in \mathcal{G}} \log q(\mathbf{x}_T | \tau) d\mathbf{x} \quad (31)$$

$$= \underset{\pi}{\operatorname{argmax}} \int_{\mathbf{x} \in \mathcal{G}} q(\mathbf{x}_T | \tau) d\mathbf{x} \quad (32)$$

which defines the probability of reaching any state in the goal set \mathcal{G} , a commonly used term for reaching a goal set in chance-constrained control (e.g. Equation (6) in [13]).

D. Maximize Probability of Reaching Goal Point

A special case of the previous result in Sec. VI-C is a Dirac-delta goal distribution $p_g(\mathbf{x}) = \delta_g(\mathbf{x})$ instead of a uniform goal distribution. We get

$$\pi^* = \underset{\pi}{\operatorname{argmax}} q(\mathbf{x}_T = \mathbf{g} | \tau) \quad (33)$$

which maximizes the probability of reaching a point-based goal \mathbf{g} following trajectory τ .

VII. PRACTICAL ALGORITHM

In this section, we formulate planning to goal distributions as a practical instantiation of our method described in Sec. V. We first describe how we compute the agent's predicted terminal state distribution with the unscented transform in Sec. VII-A. In Sec. VII-B we incorporate the unscented transform uncertainty propagation into a more concrete formulation of the constrained optimization problem defined in Eq. 1 from Sec. III. We then discuss tractable methods for computing our information-theoretic losses in Sec. VII-C. We use this formulation in our experiments in Sec VIII.

A. State Uncertainty Propagation

As noted in Sec. III, a robot typically maintains a probabilistic estimate of its state $\hat{p}(\mathbf{x}_0)$ to cope with allestoric uncertainty from its sensors and the environment [42, 89]. In order to compute the terminal state distribution $q(\mathbf{x}_T | \tau)$ and in turn compute the information-theoretic losses for Eq. 1a, we require a means of propagating the state uncertainty over the planning horizon given the initial state distribution $\hat{p}(\mathbf{x}_0)$, a sequence of actions \mathbf{U}_{T-1} , and the robot's stochastic (possibly nonlinear) dynamics function $f: \mathcal{X} \times \mathcal{U} \times \Omega \rightarrow \mathcal{X}$.

Our choice of uncertainty propagation method is informed by the evolution of nonlinear Bayesian filters [89, 95]. Perhaps the simplest method is Monte Carlo sampling, i.e. sampling initial states $\mathbf{x}_0 \sim \hat{p}(\mathbf{x}_0)$ and sequentially applying the dynamics function to acquire a collection of samples from which the terminal state distribution can be approximated. However, this approach can require thousands of samples to estimate the distribution well, which imposes a computational burden when estimating auxiliary costs and constraints (e.g. collision constraints). Other options include Taylor series approximations (akin to the extended Kalman filter) and numerical quadrature methods [95]. When the marginal state distribution is well-estimated by a Gaussian, the *unscented transform* provides an accurate estimate of the state distribution propagated under nonlinear dynamics [37] (akin to the unscented Kalman filter [91, 39]). We leverage the unscented transform in our approach since we can achieve an accurate estimate of the propagated state marginal using only a small set of deterministically computed query points without having to compute Jacobians or Hessians of the dynamics function [89].

Given a state distribution $\mathcal{N}(\mathbf{x}_t | \boldsymbol{\mu}_t, \boldsymbol{\Sigma}_t)$, the unscented transform computes a small set of *sigma points* $\mathcal{P}_t = \{\boldsymbol{\mu}_t \pm \beta \mathbf{L}_t[i]\}_{i=1}^N$ for state size N where $\mathbf{L}_t[i]$ is the i -th row of the Cholesky decomposition of the covariance $\boldsymbol{\Sigma}_t$ and β is a hyperparameter governing how spread out the sigma points are from the mean. Given an action $\mathbf{u}_t \in \mathcal{U}$, we estimate how the distribution will transform under the robot's dynamics by evaluating the noise-free dynamics function, $f(\mathbf{x}_t, \mathbf{u}_t, 0)$ at each of the sigma points $\mathbf{p}_t \in \mathcal{P}_t$ together with the action \mathbf{u}_t to get a new set of points $\mathcal{P}'_t = \{f(\mathbf{p}_t, \mathbf{u}_t, 0) | \mathbf{p}_t \in \mathcal{P}_t\}$. Taking the sample mean and covariance of the points in \mathcal{P}'_t provides an estimate of the distribution at the next timestep $\mathcal{N}(\mathbf{x}_{t+1} | \boldsymbol{\mu}_{t+1}, \boldsymbol{\Sigma}_{t+1})$. This procedure is similar to the unscented dynamics described in [37] as well as its use in unscented model predictive control [24, 93].

We assume Gaussian state distributions and use the unscented transform for uncertainty propagation in our experiments in Sec. VIII to illustrate our approach. Most popular state estimation techniques assume a Gaussian state distribution [89, 91], so this is not a particularly limiting assumption. However, we emphasize that other uncertainty propagation techniques are possible in our framework. We discuss this point further in Sec IX.

B. Planning to Goal Distributions with Unscented Transform

We now present a more concrete instantiation of the abstract optimization problem from Sec. III which we will subse-

quently use in our experiments in Sec. VIII. We formulate the optimization problem as a direct transcription of a trajectory optimization for planning to a goal distribution $p_g(\mathbf{x}_T)$ under Gaussian state uncertainty propagated by the unscented transform as described in Sec. VII-A:

$$\min_{\Theta} \mathcal{L}(\mathcal{N}(\mathbf{x}_T | \boldsymbol{\mu}_T, \boldsymbol{\Sigma}_T), p_g(\mathbf{x}_T)) \quad (34a)$$

$$+ \sum_{t=0}^{t-1} \sum_{\mathbf{p}_t \in \mathcal{P}_t} \mathcal{N}(\mathbf{p}_t | \boldsymbol{\mu}_t, \boldsymbol{\Sigma}_t) \cdot c_t(\mathbf{p}_t^i, \mathbf{u}_t) \quad (34b)$$

$$\text{s.t. } \mathbf{x}_{\min} \leq \boldsymbol{\mu}_t \leq \mathbf{x}_{\max}, \quad \forall t \in [0, T] \quad (34c)$$

$$\mathbf{u}_{\min} \leq \mathbf{u}_t \leq \mathbf{u}_{\max}, \quad \forall t \in [0, T-1] \quad (34d)$$

$$\boldsymbol{\mu}_0 = \mathbf{x}_0, \quad \boldsymbol{\Sigma}_0 = \boldsymbol{\Sigma}_{\mathbf{x}_0} \quad (34e)$$

$$\boldsymbol{\mu}_t = \frac{1}{|\mathcal{P}'_t|} \sum_{\mathbf{p}'_t \in \mathcal{P}'_t} \mathbf{p}'_t, \quad \forall t \in [1, T] \quad (34f)$$

$$\boldsymbol{\Sigma}_t = \frac{1}{|\mathcal{P}'_t|} \sum_{\mathbf{p}'_t \in \mathcal{P}'_t} (\mathbf{p}'_t - \boldsymbol{\mu}_t)(\mathbf{p}'_t - \boldsymbol{\mu}_t)^T + \mathbf{R}_t, \quad \forall t \in [1, T] \quad (34g)$$

$$\boldsymbol{\Sigma}_t \in S_{++}^N, \quad \forall t \in [0, T] \quad (34h)$$

$$g_i(\Theta) \leq 0, \quad \forall i \in [1, N_g] \quad (34i)$$

$$h_j(\Theta) = 0, \quad \forall j \in [1, N_h] \quad (34j)$$

where the decision variables Θ include the sequence of actions \mathbf{U}_{T-1} and, due to the direct transcription formulation, the sequence of means $\boldsymbol{\mu}_0, \dots, \boldsymbol{\mu}_T$ and covariances $\boldsymbol{\Sigma}_0, \dots, \boldsymbol{\Sigma}_T$ parameterizing the state distributions over the trajectory.

Eq. 34a is an information-theoretic loss between the terminal state and goal distributions. In our experiments in Sec. VIII we focus on the cross-entropy and KL divergence losses that resulted from our derivations in Sec. V-B. Eq. 34b encapsulates the arbitrary running costs from Eq. 1b, adapted here to be applied to the sigma points resulting from uncertainty propagation with the unscented transform. Note the costs are weighted by the probability of the sigma points under the predicted state distribution for the associated timestep.

Regarding constraints, Eqs. 34c and 34d are bound constraints on the decision variables. Eq. 34e ensures the initial state distribution matches the observed initial state distribution. Eqs. 34f and 34g constrain the distribution parameters at each timestep to match the empirical mean and covariance, respectively, estimated from the transformed sigma points at each timestep \mathcal{P}'_t as described in Sec. VII-A. As a reminder, $\mathcal{P}'_t = \{f(\mathbf{p}_t, \mathbf{u}_t, 0) | \mathbf{p}_t \in \mathcal{P}_t\}$ is the set of transformed sigma points under the noise-free dynamics function. The stochasticity of the dynamics is accounted for by the term \mathbf{R}_t in Eq. 34g.

Eq. 34h ensures the covariance matrices remain symmetric positive semi-definite. We note that in practice we use $\mathbf{L}_t = \text{chol}(\boldsymbol{\Sigma}_t)$ for the covariance optimization such that $\mathbf{L}_t \mathbf{L}_t^T = \boldsymbol{\Sigma}_t$, which makes it easier for optimizers to satisfy this constraint. Finally, Eqs. 34i and 34j enable us to incorporate arbitrary inequality and equality constraints on the decision variables. For example, we add collision-avoidance constraints on the sigma points computed from the distribution

parameters at each timestep in our experiments in Sec. VIII similar to [37].

C. Approximate Information-Theoretic Losses

Cross-entropy and KL divergence are two salient information theoretic losses that came out of our planning as inference derivation in Sec. V-B, and we primarily utilize these losses in our experiments in Sec. VIII. There are often closed form solutions for computing these losses (e.g. between two Gaussian distributions [38]). However, there are instances where no closed form solutions exist and approximations are necessary (e.g. between two Gaussian mixture models [35], truncated Gaussians [19]). Since we assume Gaussian state uncertainty in this article, we utilize a simple and accurate approximation where needed based on the sigma point computation discussed in Sec. VII-A. For a Gaussian distribution $p_1(\mathbf{x}) = \mathcal{N}(\mathbf{x} | \boldsymbol{\mu}, \boldsymbol{\Sigma})$ and an arbitrary distribution $p_2(\mathbf{x})$, we compute approximate cross-entropy as

$$D_{\text{CE-app}}(p_1(\mathbf{x}) \parallel p_2(\mathbf{x})) = \frac{1}{|\mathcal{P}|} \sum_{\mathbf{p} \in \mathcal{P}} -p_1(\mathbf{p}) \log p_2(\mathbf{p}) \quad (35)$$

where \mathcal{P} is the set of sigma points as discussed in Sec. VII-A. A similar approximation follows for KL divergence. These approximations are based on the unscented approximation described in [35] which demonstrated its accuracy and efficiency over Monte Carlo estimates. We utilize this approximation in our experiments when closed form solutions do not exist.

VIII. APPLICATIONS

We present several applications in which we demonstrate the utility of goal distributions as a goal representation in a planning as inference framework. In Sec. VIII-A we demonstrate some of the basic behaviors and flexibility of our approach on a simple planar navigation among obstacles problem. In Sec. VIII-B we further explore the behavior of different information-theoretic losses on an underactuated planar ball-rolling environment. We explore a more realistic scenario in Sec. VIII-C in which the agent must intercept a moving target and update its belief of the target’s location with noisy sensor readings. In Sec. VIII-D, we apply our approach to a higher dimensional problem of a 7-DOF robot arm reaching to grasp an object and uncover some intriguing benefits of a distribution-based goal in a manipulation setting. Finally, in Sec. VIII-E, we show how goal distributions naturally encode semantic goals for skill planning, and enable the use of more dynamic skills than are typically utilized in traditional skill planning approaches.

Additional details about the different solvers and environment parameters we use in this section can be found in Appendix D. All associated code² and data will be released upon acceptance.

A. Goal distributions are a flexible goal representation

We first apply our approach to a simple 2D navigation problem to highlight the flexibility of modeling task goals as goal distributions in our probabilistic planning framework. The task objective is to navigate from a start configuration to a goal while avoiding obstacles.

We emphasize that in all examples in this section, we use the same planning algorithm that we formalized in Sec. VII. Merely by changing the family and/or parameterization of the goal distribution in each example (and selecting an appropriate information-theoretic loss), we are able to plan to point-based and set-based goals as well as goals with varied models of uncertainty associated with them.

1) *Environment Description:* We use the Dubins car model from [44], a simple vehicle model with non-holonomic constraints in the state space $\mathcal{X} = SE(2)$. The state $\mathbf{x} = (p_x, p_y, \phi)$ denotes the car’s planar position (p_x, p_y) and orientation ϕ . The dynamics obey

$$\dot{p}_x = v \cos \phi, \quad \dot{p}_y = v \sin \phi, \quad \dot{\phi} = r \quad (36)$$

where $v \in [0, v_{\max}]$ is a linear speed and $r \in [-\tan \psi_{\max}, \tan \psi_{\max}]$ is the turn rate for $\psi_{\max} \in (0, \frac{\pi}{2})$. We use an arc primitive parameterization similar to [44] where actions $\mathbf{u} = (v, r)$ are applied at each timestep for duration Δt such that the robot moves in a straight line with velocity v if $r = 0$ and arcs with radius $\frac{v}{r}$ otherwise. An action sequence has the form $\mathbf{U}_{T-1} = (v_1, r_1, \dots, v_{T-1}, r_{T-1})$. We extend the model in [44] to have stochastic dynamics by adding Gaussian noise $\boldsymbol{\omega}_t \sim \mathcal{N}(\mathbf{x} | \mathbf{0}, \alpha \mathbf{I})$ to the state updates at each timestep.

We manually define a Gaussian estimate $\mathcal{N}(\mathbf{x}_0 | \boldsymbol{\mu}_0, \boldsymbol{\Sigma}_0)$ for the robot’s initial state. We compute the marginal terminal state distribution $\mathcal{N}(\mathbf{x}_T | \boldsymbol{\mu}_T, \boldsymbol{\Sigma}_T)$ using the unscented transform as described in Sec. VII-A. We use spherical obstacles and utilize the negative signed distance function (SDF) in an inequality constraint $-d_{\text{SDF}}(\mathbf{x}_t, \mathbf{o}_i, r_i) \leq 0$ for all timesteps $t \in [0, T]$ where $T = 45$ is the planning horizon and (\mathbf{o}_i, r_i) are the origin point $\mathbf{o}_i \in \mathbb{R}^2$ and radius $r_i \in \mathbb{R}$ of a spherical obstacle. These constraints apply to the mean trajectory as well as the computed sigma points at each timestep as described in Sec. VII-B.

2) *Navigating to a goal region:* We define the goal region \mathcal{G} as the blue, hatched rectangle shown in Fig. 2a. We are able to plan directly to this region by modeling it as a uniform goal distribution $p_g(\mathbf{x}_T) = \mathbb{U}_{\mathcal{G}}(\mathbf{x}_T)$. Here we utilize the M-projection of the cross-entropy loss $D_{\text{CE}}(\mathbb{U}_{\mathcal{G}}(\mathbf{x}_T) \parallel \mathcal{N}(\mathbf{x}_T | \boldsymbol{\mu}_T, \boldsymbol{\Sigma}_T))$ since the uniform distribution has finite support as discussed in Sec. IV-B and Sec. V-B4. As a reminder, this objective is equivalent to the chance-constrained goal set objective [13] as discussed in Sec. VI-C. The resulting plan is shown in Fig 2a, where the orange dotted line shows the planned mean path of the robot and the orange ellipses show two standard deviations of the robot’s predicted Gaussian state uncertainty over the trajectory. This result demonstrates our probabilistic planning framework accommodates traditional set-based goal representations. In contrast to traditional planning approaches that sample a particular point $\mathbf{g} \in \mathcal{G}$ from the set \mathcal{G} to plan to [52], we are able to plan directly to the region.

²A preliminary release of our code can be found here:

https://bitbucket.org/robot-learning/distribution_planning

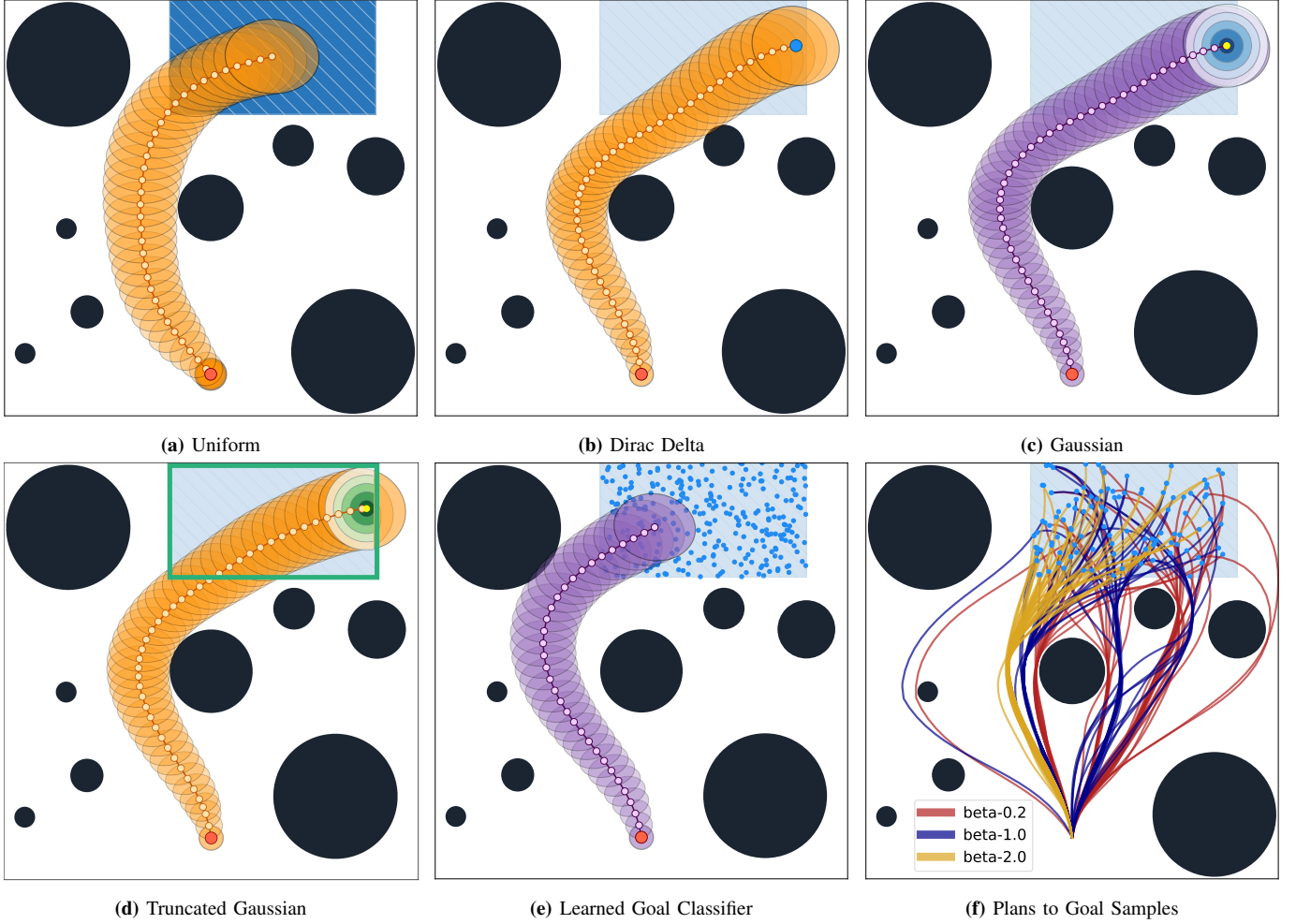


Fig. 2: Examples of planned paths with our probabilistic planning framework on a 2D navigation environment. In each figure, the robot starts at the red dot and must navigate to a goal while avoiding obstacles (black spheres). Planned mean paths (dotted lines) and the associated predicted covariance (ellipses) are shown. Orange paths were solved with the M-projection of cross-entropy and purple paths were solved with the I-projection of cross-entropy. (a) A goal set modeled as a uniform distribution (blue, hatched rectangle). (b) A goal point modeled as a Dirac-delta distribution (blue dot). (c) A Gaussian goal distribution (yellow dot is mean, blue ellipses are standard deviations of covariance). (d) A truncated Gaussian goal where the PDF is Gaussian inside the green rectangle and zero outside of it. (e) A goal classifier learned from goal samples (blue dots). (f) Plans to particular goal points (Dirac-delta distributions) using values $\beta = 0.2$ (red lines), $\beta = 1.0$ (blue lines), and $\beta = 2.0$ (yellow lines).

While we are able to plan directly to the goal region \mathcal{G} as just described, we can also plan to any particular point $g \in \mathcal{G}$ (blue dot in Fig 2b) by modeling the goal point as a Dirac-delta distribution $p_g(x_T) = \delta_g(x_T)$ as discussed in Sec. IV-A. We again use the M-projection cross-entropy loss $D_{CE}(\delta_g(x_T) \parallel \mathcal{N}(x_T \mid \mu_T, \Sigma_T))$ due to the finite support of the Dirac-delta distribution. As a reminder, this objective amounts to maximizing the probability of reaching a goal point (Sec. VI-D). We show the resulting plan for reaching this arbitrarily, sampled point in Fig 2b. This results shows that we retain point-based and set-based goal representations in our probabilistic framework.

We depart from traditional set-based and point-based goal representations in Fig. 2c with a Gaussian goal distribution $p_g(x_T) = \mathcal{N}(x_T \mid \mu_g, \Sigma_g)$ as described in Sec. IV-C. The Gaussian distribution has infinite support and therefore we use the I-projection of cross-entropy

$D_{CE}(\mathcal{N}(x_T \mid \mu_T, \Sigma_T) \parallel \mathcal{N}(x_T \mid \mu_g, \Sigma_g))$. The resulting plan is shown in Fig. 2c. We set the mean of the Gaussian to the same point sampled from the previous example for comparison. We note that in this particular unimodal example, the M-projection plan looks similar. This result demonstrates we are able to generate plans to a goal location while explicitly accounting for the robot’s Gaussian belief about which goal point it should navigate to.

We additionally consider a truncated Gaussian goal distribution $p_g(x_T) = \mathcal{N}(x_T \mid \mu_g, \Sigma_g, \mathcal{G})$ shown in Fig. 2d. We choose the same Gaussian distribution as in the previous example, but bound the PDF to the goal region \mathcal{G} as illustrated by the green rectangle in Fig. 2d such that the PDF is equal to zero outside the goal region. As discussed in Sec. IV-C, this serves as a model of bounded uncertainty in which the agent has Gaussian uncertainty about a point-based goal in the goal region, but the well-defined goal region

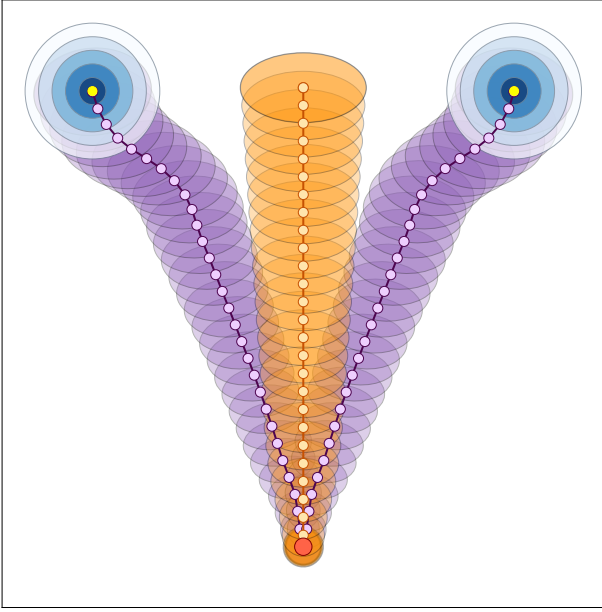


Fig. 3: A two-component Gaussian mixture model goal distribution. Yellow dots indicate the two modes of goal distribution and blue ellipses show standard deviations of the goal covariance. We show two I-projection paths (purple paths, one to each component) and one M-projection path (orange path). Purple and orange ellipses show the associated state uncertainty for the respective paths.

limits the agent’s belief to be contained within the goal region. Note we again use the M-projection of cross-entropy $D_{CE}(\mathcal{N}(x_T | \mu_g, \Sigma_g, \mathcal{G}) \parallel \mathcal{N}(x_T | \mu_T, \Sigma_T))$ since the truncated Gaussian has finite support. We also note we use the approximate cross-entropy discussed in Sec. VII-C since there is no closed form solution for truncated Gaussians.

We now consider a goal classifier learned from data as shown in Fig. 2e. The blue dots indicate samples that are considered goals. We acquire negative samples by sampling uniformly from the environment region outside the goal region. We train a simple neural network model $f(x; \theta)$ consisting of fully connected layers with ReLU activations. We utilized two hidden layers of width 32 and trained the model with binary cross-entropy loss. We again utilize the approximate cross-entropy loss from Sec. VII-C. As discussed in Sec. IV-F, this is a very general goal representation that can model complex goals, and we can use it directly as a goal in our planning framework.

For our last example in this section, we show several plans to different point-based goals (i.e. Dirac-delta distributions) with varying values of the β parameter discussed in Sec. VII-A. The β parameter governs how spread out the sigma points get in propagating state uncertainty with the unscented transform. Since we apply collision costs to the sigma points, the beta parameter in this environment determines how closely the agent will navigate to obstacles. As shown in Fig. 2f, a value of $\beta = 0.2$ results in more aggressive plans that navigate closer to obstacles while a value of $\beta = 2.0$ generates plans that keep a wider berth away from obstacles. Plans for $\beta = 2.0$ all take a similar route since that is the only homotopy solution class for this environment that does not result in sigma point

collisions. Simply by lowering the value of beta, we start getting paths in different homotopy classes that can safely maneuver through more narrow gaps between obstacles. We note that the variation in solutions largely comes from the initial solution provided to the solver. Thus, seeding the solver differently can result in paths from different homotopy classes even when planning to the same goal.

3) I-projection vs. M-projection for multimodal goal:

We now look at a Gaussian mixture model (GMM) goal distribution $p_g(x_T) = \mathcal{M}(x | \{\alpha_i, \mu_i, \Sigma_i\}_{i=1}^M)$ as defined in Sec. IV-E. In contrast to the unimodal example from Fig. 2c, the I-projection and M-projection of cross-entropy for a multimodal GMM exhibit notably different behavior as shown in Fig. 3. As discussed in Sec. V-B4, the I-projection is mode-seeking and thus is capable of generating plans to either mode depending on the parameter initialization provided to the solver. We show one instance of a plan to each GMM mode in Fig. 3 (purple paths). The M-projection exhibits moment-matching behavior and will strive to concentrate the mass of the terminal state distribution to cover all modes of the goal distribution. The M-projection results in a plan that terminates in between the two modes of the goal distribution (orange path in Fig. 3). This is a well-known feature of the information and moment projections for multimodal distributions [65]. However, we find it insightful to demonstrate this behavior in our probabilistic planning framework. In most planning problems it is desirable to optimize to a particular mode, and thus the I-projection will be preferred. However, there are instances where the M-projection may be desirable for a multimodal distribution, e.g. surveillance or allocation problems that require an agent to be in proximity to several targets simultaneously [7].

B. Goal distributions enable leveraging sources of uncertainty for planning

In Sec. V-A, we showed that both cross-entropy and KL divergence are meaningful information theoretic losses when planning to goal distributions from the perspective of planning as inference. The examples in Sec. VIII-A did not have notable differences between cross-entropy and KL divergence. This is because in the M-projection cases, the entropy of the goal distribution is constant in the optimization and thus minimizing cross-entropy and KL divergence are equivalent. For the I-projections, the terminal covariance is largely determined by the horizon of the plan, since we only considered homogeneous dynamics noise over the environment. We now consider an example with heteroscedastic noise that shows a clear difference between these two objectives, and compare also to point-based planners.

We consider a 2D ball-rolling environment (pictured in Fig. 4) in which the agent must select the initial position and velocity of a ball such that the ball will end up as close to a target location as possible. Note that in contrast to the previous environment, the agent only applies control input at the initial timestep and must leverage the passive dynamics of the environment to get the ball to the desired target location.

We use the state and dynamics model of [92]. The state space $\mathcal{X} \subseteq \mathbb{R}^6$ consists of the planar position p , velocity $v =$

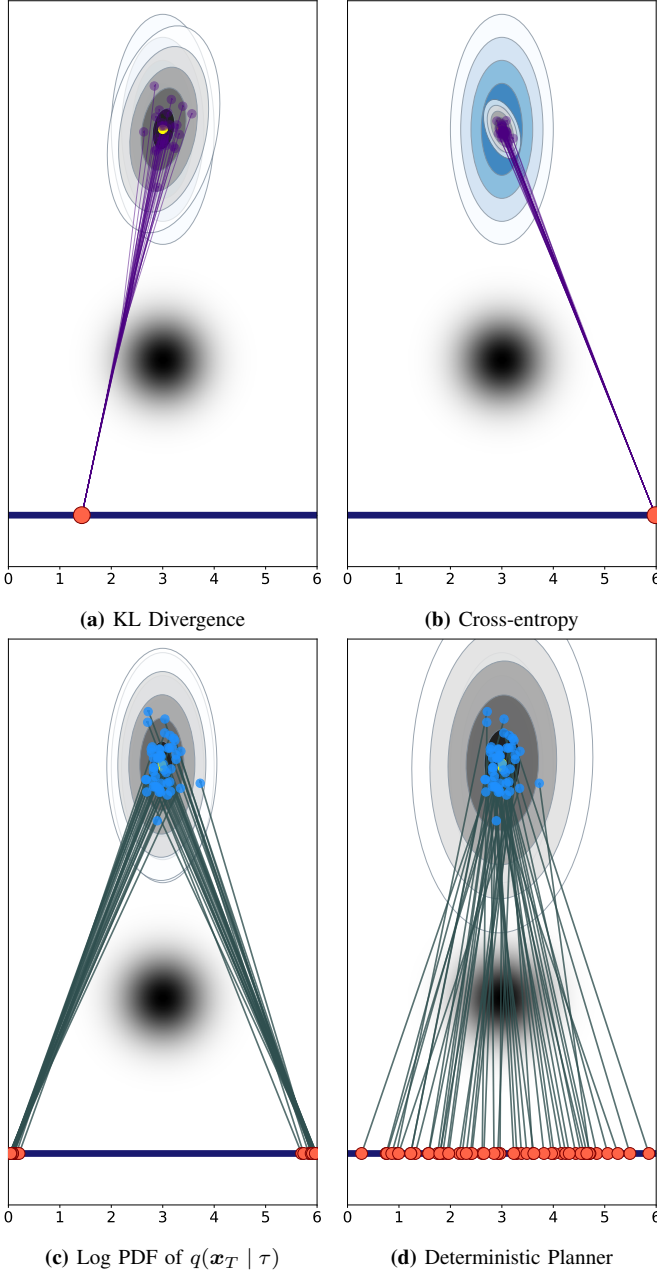


Fig. 4: Comparison of different planning objectives for a 2D ball-rolling environment. The initial ball position (red dot) is constrained to the dark blue line. Blue ellipses denote the Gaussian goal distribution. Grey ellipses illustrate the terminal state distribution fitted from rollouts. The black gradient is a noise amplifier that increases dynamics noise the closer the ball gets to darker-colored regions. **(a)** KL divergence plans leverage the additional noise uncertainty from the amplifier to more closely match the terminal covariance of the goal distribution. Purple lines show paths from 20 rollouts of the plan. **(b)** Cross-entropy plans avoid the noise amplifier and achieve a tight covariance about the goal mean. **(c)** Using the negative log PDF of the terminal state distribution as the cost, we plan to 50 samples from the goal distribution (blue dots) and avoid the noise amplifier. Lines indicate the planned path for the 50 different goal samples. **(d)** A deterministic planner ignores the noise amplifier in planning to the goal samples, resulting in a terminal distribution that does not match the goal distribution.

$\dot{\mathbf{p}}$, and acceleration $\mathbf{a} = \ddot{\mathbf{p}}$ of the ball. The acceleration of the ball is computed by $\mathbf{a} = \mathbf{F}/m$ where $m = 0.045\text{kg}$ is the mass of the ball in kilograms and the force

$$\mathbf{F} = -\mu_f \|\mathbf{N}\| \frac{\mathbf{v}}{\|\mathbf{v}\|} \quad (37)$$

is the frictional force applied to the ball from the ground where μ_f is the coefficient of friction and \mathbf{N} is the normal force applied to the ball from the ground. We assume a flat surface so that the normal force is simply counteracting gravity, i.e. $\mathbf{N} = (0, 0, mg)$ for $g = 9.8\text{m/s}^2$. We use a friction coefficient of $\mu_f = 0.04$. We compute velocity and position using Euler integration from the computed acceleration with a timestep of $dt = 0.3$. We constrain the position to the blue line shown in Fig. 4.

We apply a small additive isotropic Gaussian noise $\omega \sim \mathcal{N}(\mathbf{a} | \mathbf{0}, \alpha \mathbf{I})$ to the acceleration for $\alpha = 0.0001$. However, this environment has heterogeneous noise. The black, circular gradient shown in Fig. 4 is a noise amplifier defined by a Gaussian distribution that adds an additional $\omega' \sim \mathcal{N}(\mathbf{a} | \mathbf{0}, \alpha' \mathbf{I})$ where α' is proportional to the Mahalanobis distance between the agent and the center of the noise amplifier. Intuitively, the closer the ball gets to the center of the noise amplifier, the more dynamics noise is added to the acceleration. This behavior mimics exacerbated state uncertainty induced by the environment, e.g. a patch of ice.

We consider a Gaussian goal distribution $p_g(\mathbf{x}) = \mathcal{N}(\mathbf{x} | \mu_g, \Sigma_g)$ illustrated by the blue ellipses in Fig. 4. We again use the unscented transform to compute the marginal terminal state distribution $\mathcal{N}(\mathbf{x}_T | \mu_T, \Sigma_T)$. In order to compare the terminal distributions resulting from each plan, we run a total of 500 rollouts per trial and fit a Gaussian distribution to the points at the last timestep using maximum likelihood estimation. Terminal distributions are visualized by grey ellipses in Fig. 4 showing standard deviations. Note we estimate the terminal distributions using rollouts instead of the unscented transform prediction in order to put the comparison on an even footing with the deterministic point-based planner we will discuss shortly, which has no associated method of uncertainty propagation.

As shown in Fig. 4a, minimizing the I-projection of KL divergence $D_{\text{KL}}(\mathcal{N}(\mathbf{x}_T | \mu_T, \Sigma_T) \parallel \mathcal{N}(\mathbf{x}_T | \mu_g, \Sigma_g))$ results in a plan that has the ball pass close by the noise amplifier. The terminal distribution matches the goal distribution with a KL divergence value of 0.796. However, minimizing the I-projection of cross-entropy $D_{\text{CE}}(\mathcal{N}(\mathbf{x}_T | \mu_T, \Sigma_T) \parallel \mathcal{N}(\mathbf{x}_T | \mu_g, \Sigma_g))$ results in a plan that avoids the noise amplifier and keeps a tight covariance for the terminal state distribution as shown in Fig. 4b. The resulting distribution has a KL divergence value of 2.272 with respect to the goal distribution. This higher KL divergence value is due to cross-entropy seeking to maximize the expected (log) probability of reaching the goal, which incentivizes a lower entropy terminal state distribution. This is evident when we consider that $D_{\text{CE}}(p_1 \parallel p_2) = \mathcal{H}(p_1) + D_{\text{KL}}(p_1 \parallel p_2)$ as discussed previously in Sec. V-B3.

We further consider two point-based planners. First, we use the negative log probability of the computed terminal state

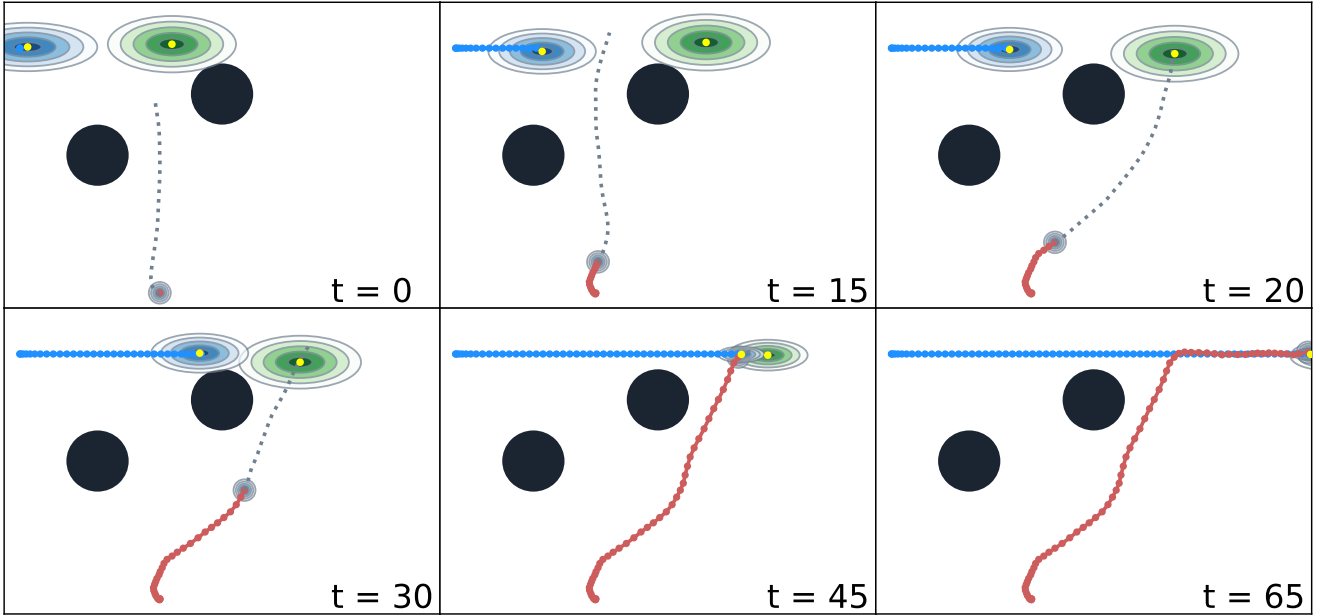


Fig. 5: A selection of frames from an MPC execution of a planar navigation agent intercepting a moving target. The actual goal path is denoted by the blue line, the blue ellipses display the agent’s Gaussian belief about where the goal is at each timestep, and the green ellipses display the agent’s projected Gaussian belief of where the goal will be at the end of the planning horizon. The agent’s path is denoted by the red line in each frame, and the gray dotted line displays its current plan. Dark spheres are obstacles to avoid. See Sec. VIII-C for details.

distribution $\mathcal{N}(x_T \mid \mu_T, \Sigma_T)$ as the cost. We sample 50 goal points from the Gaussian goal distribution (blue dots in Fig. 4c) and generate a plan for each goal point. We perform 10 rollouts for each of the 50 plans for a total of 500 rollouts and fit the Gaussian distribution displayed with grey ellipses in Fig. 4c. We see that the terminal distribution matches very closely to the goal distribution with a KL divergence of 0.770. This value is only slightly lower than the distribution we achieved with 500 rollouts of the single plan resulting from optimizing KL divergence. Second, we consider a deterministic planner that plans to each of the goal samples and assumes there is no noise in the dynamics. As shown in Fig. 4d, we get solutions where the initial position of the ball is spread out over the range of the start region. Some of the plans then have the ball pass directly over the noise amplifier, resulting in rollouts that may disperse the ball far away from its target location. We again perform 10 rollouts for each of the 50 plans and find the terminal Gaussian distribution to have a KL divergence of 1.388, nearly double the value of the KL divergence plan and log probability plans. It is therefore not sufficient to deterministically plan to sample points from the goal distribution, and we achieve better results utilizing the predicted terminal state uncertainty. Note that with the point-based planners, we must compute a separate plan for every point. In contrast, we computed a single plan optimizing KL divergence that resulted in a terminal state distribution closely matching the goal distribution.

These examples illustrate that our framework is able to advantageously leverage sources of uncertainty in the environment to achieve a target state distribution. We note similar results can also be achieved in environments with

homogeneous noise if the agent optimizes stochastic policies, e.g. with reinforcement learning.

C. Goal distributions enable belief updates for moving targets

We have so far only considered examples with static goal distributions. We now consider a more realistic scenario in which the goal distribution changes over time and is updated based on the agent’s observations. The robot’s task is to intercept a moving target while maintaining a Gaussian belief of the target’s location from noisy observations.

We use the widely utilized double integrator system [77, 50] for both the agent and the moving target in a planar environment. The agent’s state space $\mathcal{X} \subseteq \mathbb{R}^4$ consists of a planar position $\mathbf{p} \in \mathbb{R}^2$ and velocity $\mathbf{v} \in \mathbb{R}^2$ and the action space $\mathcal{U} \subseteq \mathbb{R}^2$ is the agent’s acceleration $\mathbf{a} \in \mathbb{R}^2$. The dynamics obey $\mathbf{v} = \dot{\mathbf{p}}$ and $\mathbf{a} = \dot{\mathbf{v}}$ and we compute the position and velocity through double Euler integration of the applied acceleration (hence the name “double integrator”).

The agent maintains a Gaussian belief of the target’s location (blue ellipses in Fig. 5) that is updated at every timestep using a Kalman filter [40]. The agent also uses the Kalman filter to project its Gaussian belief of the target’s location over the planning horizon to represent the agent’s Gaussian belief of the target’s future location (green ellipses in Fig. 5). Note that the target moves deterministically in a straight line with constant velocity from left to right. The agent uses this motion model in the Kalman updates, but assumes the agent moves stochastically. The agent receives noisy observations of the target’s location at every timestep, where the observations get more accurate the closer the agent gets to the target.

We use the I-projection of cross-entropy as our planning objective. We interleave planning and control with a model predictive control (MPC) scheme. The agent creates a plan for a small horizon, executes the first action of the plan in the environment, acquires an observation from the environment, and then re-plans. This procedure continues until a termination condition is achieved. We use *model predictive path integral control (MPPI)* as our plan update procedure. MPPI is a sampling-based solver that is widely used due to its computation efficiency and efficacy on complex domains. See Appendix D-C for details on the solver and MPC scheme we use.

We see in Fig. 5 that initially (timesteps $t = 0$ and $t = 15$) the agent plans a path between the two obstacles to the projected goal distribution. However, as the target advances in its trajectory, the agent gets new observations that push the projected goal distribution far enough along that the agent starts planning paths that go to the right of all obstacles (starting at $t = 20$). The agent thus switched the homotopy class of its planned path to better intercept the target based on its prediction.

By timestep $t = 45$, the agent has intercepted the target. Note that the agent’s uncertainty at this point is much lower than earlier in the execution (denoted by the smaller ellipses for the Gaussian belief in Fig. 5). This is due to the observation model we define that enables the agent to incorporate more accurate observations into the Kalman filter state estimation as the agent gets closer to the target. Once the agent intercepts the target ($t = 45$), it continues to move along in sync with the target, as shown in the final frame of Fig. 5 for $t = 65$. Note that the agent’s path does not precisely follow the target but deviates slightly. This is due to the agent executing with stochastic dynamics, and there is some irreducible uncertainty about where the target is located due to the alleotric uncertainty of the agent’s sensors.

This example demonstrates an application of our approach to a more realistic setting in which the agent must update its belief of its goal online using noisy observations. Importantly, we were able to use the output of a Kalman filter directly as our goal representation for planning, as opposed to only using the mean or a sample from the belief distribution. We only explored the I-projection of cross-entropy in this simple example. However, we believe other objectives (e.g. the M-projection) discussed in our planning framework deserve more detailed attention, a point we discuss further in Sec. IX.

D. Goal distributions are a better goal representation for robot arm reaching

We now turn to a more complex domain than the previous experiments to demonstrate an advantage of a distribution-based goal over a point-based goal. We address the problem of a 7-DOF robot arm reaching to grasp an object [18, 60] shown in Fig. 6. The objective for the robot is to reach its end-effector to a pre-grasp pose near an object such that closing the fingers of the hand would result in the robot grasping the object.

A common heuristic for generating pre-grasp pose candidates is to select poses that align the palm of the hand to a

face of an axis-aligned bounding box of the object [57, 58, 63]. Zero-mean Gaussian noise may also be added to each candidate to induce further variation in the pose candidates [57]. We model this explicitly as a mixture of distributions (Sec. IV-E) where each component is a distribution over SE(3) poses. We represent each SE(3) pose distribution as a Gaussian distribution (Sec. IV-C) over the 3D position together with a Bingham distribution (Sec. IV-D) over the SO(3) orientations of the end-effector. We refer to this distribution as a *pose mixture model*. The distribution is defined relative to the object, and therefore as the object is placed in different locations on the table shown in Fig. 6, the goal distribution is transformed to the object’s reference frame. This distribution is similar to the Gaussian mixture model used to encode goals fit from data for object-reaching in a learning from demonstration setting in [18]. However, our pose mixture model is more correct in the sense we properly model the distribution of orientations as a Gaussian distribution in SO(3).

We use the simulated 7-DOF KUKA iiwa arm shown in Fig. 6 with state space $\mathcal{X} \subset \mathbb{R}^7 \times \text{SE}(3)$ consisting of joint positions $\mathbf{q} \in \mathbb{R}^7$ in radians together with the pose of the end-effector $\mathbf{p} \in \text{SE}(3)$. We use quaternions to represent the end-effector orientation which naturally pairs with our use of the Bingham distribution as described in Sec. IV-D. The robot’s action space $\mathcal{U} \subset \mathbb{R}^7$ consists of changes in joint angles $\Delta\mathbf{q} \in \mathbb{R}^7$. The state transition dynamics are governed by

$$\mathbf{q}_{t+1} = \mathbf{q}_t + \Delta\mathbf{q}_t \quad (38)$$

$$\mathbf{p}_{t+1} = FK(\mathbf{q}_{t+1}) \quad (39)$$

where $FK(\cdot)$ is the robot’s forward kinematics. An Allegro hand is mounted on the robot arm. The robot’s objective is to orient the palm link of the hand to a pre-grasp pose. We use a fixed grasp pre-shape joint configuration for the fingers. We use the “sugar box” object from the YCB dataset in our experiments, shown in Fig. 6. We defined a goal pose mixture model with 6 components following the heuristic from [57].

This problem is traditionally solved by selecting a particular point-based goal to create a motion plan for [57]. For example, we can generate a sample from the pose mixture model we have defined. However, many of the samples will be unreachable based on the kinematics of the robot arm. A target pose relative to the object may be reachable when the object is placed in some poses on the table, and unreachable in others. We quantify this for our environment by spawning the object in 100 random locations on the table. We then generate 100 samples from the pose mixture model distribution and use the robot’s inverse kinematics (IK) to compute joint configurations that would enable the robot to reach to each sample. A sample is considered reachable if an IK solution can be found for that sample, and unreachable otherwise. We use Drake [88] to compute IK solutions, where we make up to 10 attempts to find a solution, each time seeding the solver with a different joint configuration sampled uniformly within the robot’s joint limits.

We find that for the 100 random poses of the object, a mean value of 39.53 of the 100 generated samples are unreachable with a standard deviation of 16.97. We additionally quantify

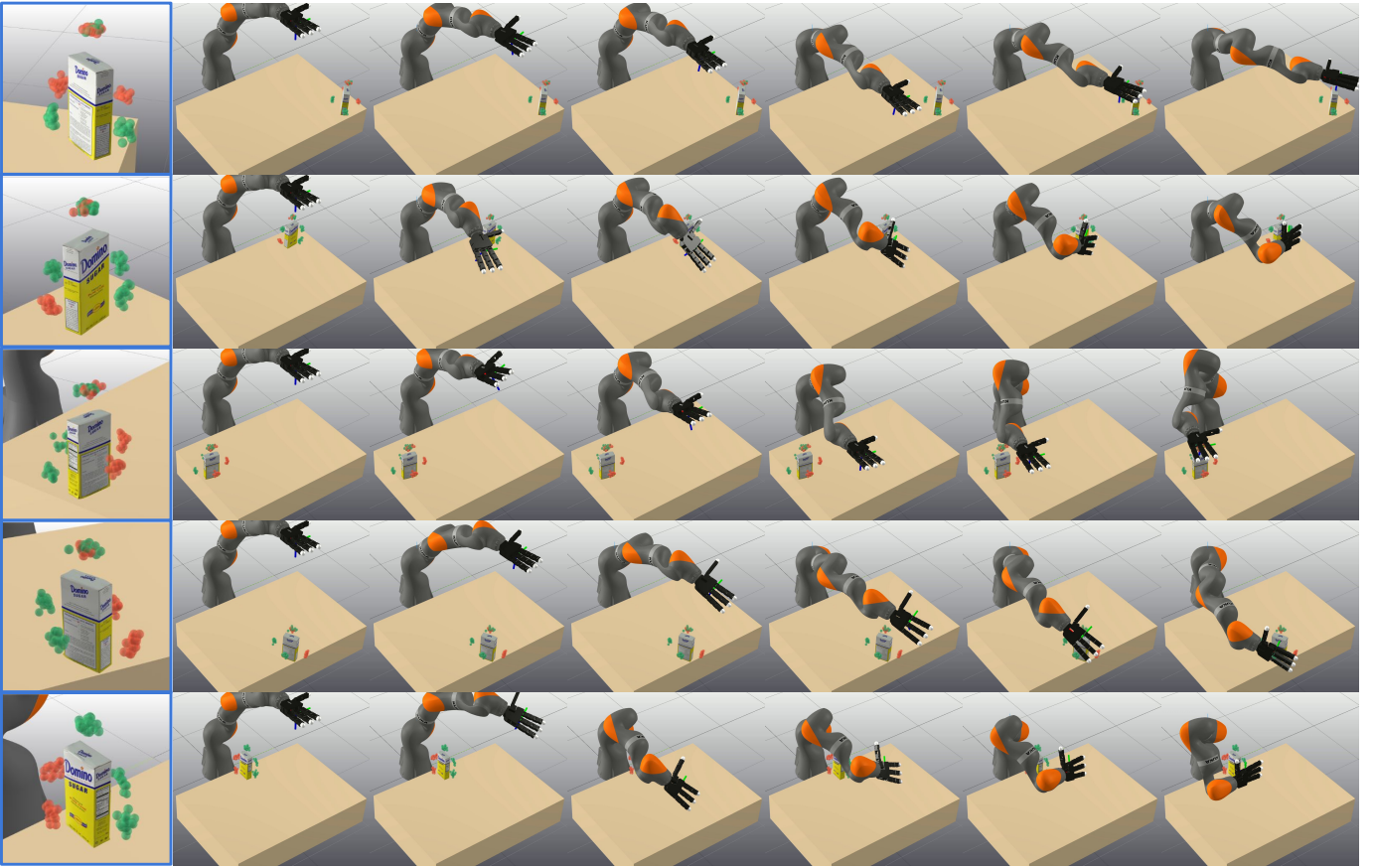


Fig. 6: Examples of a 7-DOF arm reaching its end-effector to a goal pose mixture model distribution about an object to be grasped. Close-up views of the object are shown in the first frame in each row, where green and red spheres indicate whether a pose is reachable or not, respectively. Each row shows the reaching motion where time increases from left to right.

the number of unreachable components per object pose by generating 100 samples from each component. We determine a component to be unreachable if at least 50 of the 100 component samples are unreachable. We find that on average 2.38 of the 6 components are unreachable with a standard deviation of 1.08 (see Appendix C for more visualizations of reachability). These numbers suggest that simply generating goal samples for a point-based planner will frequently result in goal points that are not feasible (i.e. unreachable). The point-based planner will therefore need to first validate the point is reachable by computing inverse kinematics prior to planning.

Using our probabilistic planning approach and the pose mixture model as the goal distribution, we are able to generate reaching plans without having to check for reachability with inverse kinematics. A selection of executions are shown in Fig. 6. We define a pose distribution for the end-effector with a fixed covariance which we transform over the planning horizon to mimic uncertainty propagation. We make this simplification since the dynamics noise on industrial robot arms like the KUKA iiwa we utilize is typically negligible. We note that proper uncertainty propagation can be performed using unscented orientation propagation [29]. We use the approximate cross-entropy loss described in Sec. VII-C since there is no closed form solution between a pose distribution and pose mixture model.

We ran our approach 10 times on all 100 object poses, each time with a different seed for random number generators, to quantify how often the plans reach to a reachable component, where component reachability is determined as described above. Our approach reaches to a reachable component with a mean percentage of 96.4% and standard deviation of 2.059% over the 10 trials. The instances where our approach does not plan to a reachable component are due to the solver getting stuck in local optima. This effect could be mitigated by a more advanced solver, e.g. using Stein variational methods [50].

In summary, a pose mixture model is a common heuristic representation for target pose candidates in reaching to grasp an object. Instead of planning to point-based samples, our approach is capable of using the pose mixture model distribution directly as the goal representation. In contrast to the point-based goal representation, we do not have to compute inverse kinematics to first determine if the target pose is reachable or not.

E. Goal distributions are a better goal representation for planning with dynamic skills

All of the applications we have looked at so far have had state dynamics that were well-captured by analytic functions. In our final application, we investigate planning to goal distributions in the domain of manipulation skill planning where

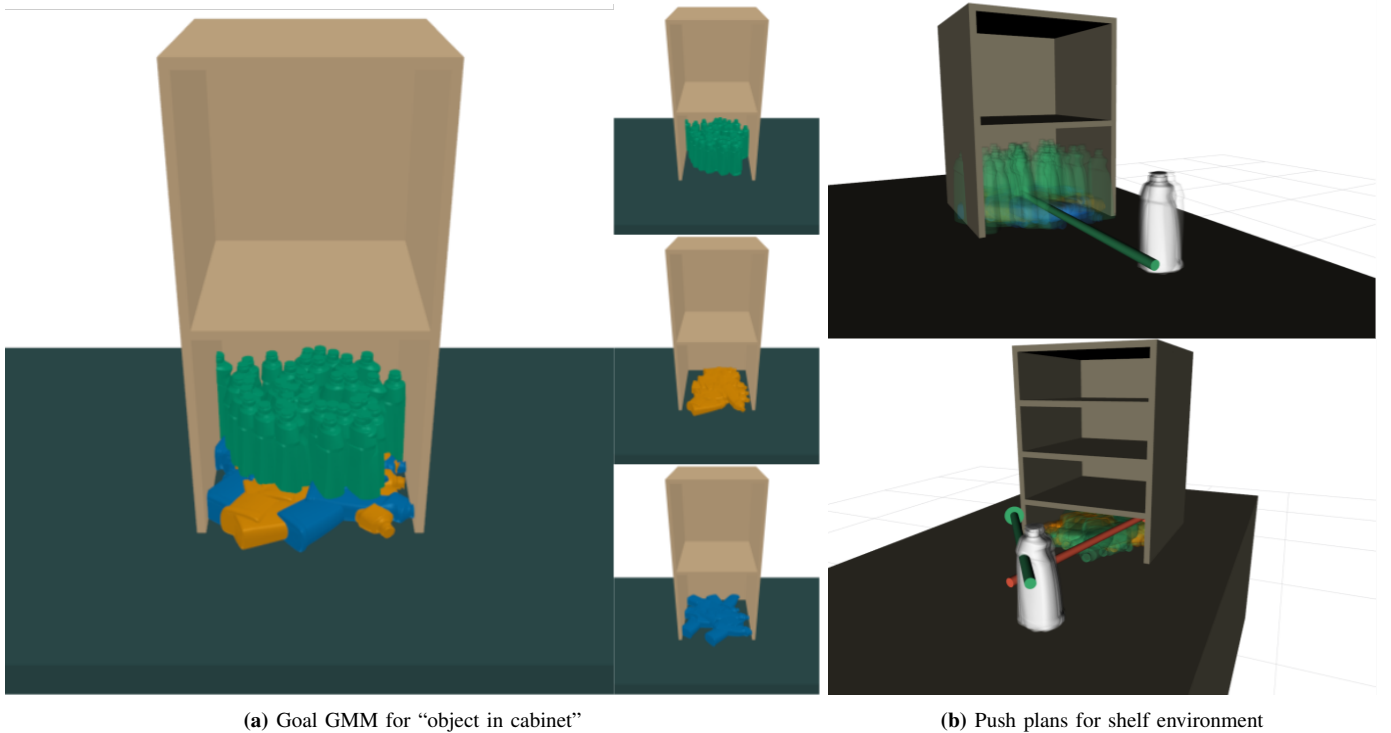


Fig. 7: Goal distribution and push plans generated by our planner for the task of relocating an object (cleaner bottle from YCB [14] dataset) to a nearby cabinet. **(a)** Goal GMM for the goal of “object in cabinet” capturing the semantic ambiguity of the goal such that the object can be placed in any pose within the cabinet, either upright (green) or on one of its flat supporting side surfaces (orange and blue). **(b)** One-step (upper) and two-step (lower) push-plans generated by our planner. The one-step plan (green arrow) is a low-push that slides the object into the cabinet, where the shelf is high enough that the upright object fits under the shelf. The two-step plan first executes a high-push (green arrow) to topple the object onto its side, and then executes a low-push (red arrow) to relocate the object into the cabinet. The topple-then-relocate approach is necessary since the lower shelves prevent the upright object from being directly relocated to the cabinet with a single push.

a learned dynamics function is necessary for good planning performance. We show how a learned dynamics function can be utilized in our framework and demonstrate how goal distributions naturally encode the uncertainty inherent to goals for manipulation tasks.

Manipulation skill planning requires a robot to determine how to sequence primitive skills (e.g. push, pick-place) from a set of skills \mathcal{S} in order to manipulate its environment into a desired configuration. We will consider the concrete example shown in Fig. 7 in which the robot is tasked to relocate an object from a kitchen counter to a nearby shelf. Each skill has an associated set of parameters Θ_k that determine how the skill is executed. For example, a push skill might be parameterized by start and end poses of the end-effector. Skill planning thus requires the robot to find a sequence of skills $S_1, \dots, S_m \in \mathcal{S}^m$ as well as the associated parameters for each skill $\theta_1, \dots, \theta_m$ such that the desired outcome is achieved when the sequence is executed.

Skill planning is traditionally formulated with point-based goals [27, 83]. However, goals for manipulation tasks often have inherent uncertainty due to semantic ambiguity and partial observability which is not captured by a point-based goal representation. For example, the goal “object on shelf” is satisfied irrespective of the particular pose the object is in on the shelf. If there are multiple shelves in the scene, the goal may also be satisfied irrespective of the particular

shelf the object is on. The robot may also have uncertainty about where the object is located, e.g. due to occlusion by other objects in the scene. These scenarios are nicely encoded by mixture models as discussed in Sec. IV-E, e.g. Gaussian mixture models. Goal distributions are therefore an excellent goal representation to accommodate the various sources of uncertainty a robot faces in manipulation tasks.

In order to address skill planning in our probabilistic planning framework, we require a dynamics function to propagate the state uncertainty. Traditionally, skill planning methods utilize skills that obey quasi-static dynamics [83]. This assumption allows for dynamics models that assume the skill is executed perfectly and that the outcome of the skill can be easily predicted as a single point in state space using a learned skill effect model [56]. However, more dynamic skills such as toppling, shoving, and tossing have aleatoric uncertainty due to the complex contact dynamics between interacting objects. This makes accurate skill outcome prediction infeasible for point-based predictors. For example, it is intractable to predict precisely where a dropped bottle will come to rest. With this intuition in mind, we learn probabilistic skill effect models, a probabilistic variant of the skill effect models (SEMs) described in [56] that predict the outcome of a skill. We consider a model for a skill $S_k \in \mathcal{S}$ that predicts $\omega_{t+1} = f_k(\omega_t, \theta, \xi_k)$, where $\omega_t \in \Omega_{\mathcal{X}}$ encodes a probability distribution over states at time t , $\omega_{t+1} \in \Omega'_{\mathcal{X}}$ encodes a probability distribution

over states at time $t + 1$, $\theta \in \Theta_k$ are skill parameters, and $\xi_k \in \Xi_k$ are function parameters (e.g., neural network weights). Intuitively, probabilistic SEMs predict how a state distribution will transform after applying skill $S_k \in \mathcal{S}$ using parameters $\theta_k \in \Theta_k$. Examples of uncertainty parameters $\Omega_{\mathcal{X}}$ include sufficient statistics of a distribution (e.g., mean and covariance of a Gaussian distribution) or Dirac measures over the state space.

Our probabilistic SEMs predict the state uncertainty induced by a single skill execution. In order to enable multi-step skill planning, we require a method to chain our predictions to predict the terminal state distribution, as described in Sec. VII. While the unscented transform was sufficient for the previous applications we investigated, we require a more general method of uncertainty propagation for SEMs since the predictions are not restricted to be Gaussian. We employ a simple strategy that is widely applicable to arbitrary distribution models based on Markov chain Monte Carlo (MCMC) sampling. We consider SEMs that have an input space $\Omega_{\mathcal{X}}$ of Dirac-delta measures (i.e., point-based inputs), an arbitrary output space $\Omega'_{\mathcal{X}}$, and we define $g : \Omega'_{\mathcal{X}} \rightarrow \Omega_{\mathcal{X}}$ to be a function that generates samples $x_t \sim \omega_t$ from the distribution $\omega_t \in \Omega'_{\mathcal{X}}$. For each step in the plan, we sample a state $x_t \sim \omega_t$, input that point to the SEM to predict $\omega_{t+1} = f_k(x_t, \theta_t, \xi_k)$, and continue in this fashion chaining the model predictions until we acquire a predicted terminal state x_T for the sample sequence. We then repeat this procedure for an arbitrary number of samples from the initial state distribution ω_0 to collect a set of predictions for the terminal state $\{x_T^i\}$. Finally, we compute the terminal distribution $q(x_T | \omega_0, \theta_1, \dots, \theta_{T-1})$ by fitting the distribution to the sample set $\{x_T^i\}$ in a maximum likelihood fashion.

We now have all of the pieces required to apply our probabilistic planning framework to skill planning under uncertainty with dynamic skills. To demonstrate the applicability of our method in this context, we consider the task of relocating a bottle sitting on a table to a nearby cabinet with shelves, shown in Fig. 7. We equip the robot with a simple pushing skill parameterized by the start and end poses of the robot’s end-effector in the coordinate frame of the object. Importantly, depending on the height at which the robot pushes the bottle, the bottle may remain upright and slide or it may topple over. The terminal pose of the bottle is therefore difficult to predict with a point-based model since it may rotate and bounce once it is pushed (see Appendix E for more details).

For our application, we use mixture density networks (MDNs) [12]: given an object pose as input, we predict the parameters of a Gaussian mixture model (GMM) over the resulting change in object pose. We found GMMs to best model scenarios with bifurcating dynamics, e.g. pushing the bottle at half its height might result with the object remaining upright or toppling over depending on subtle differences between skill executions (see Appendix E for model comparisons). We trained the model with 10,000 instances of the robot pushing the bottle with an engineered, motion-planned behavior. We used the NVIDIA Isaac Gym simulator to parallelize data collection. Please see Appendix E for further details on the specific model architecture, data collection, and

training procedure we utilized.

We use Gaussian mixture models (GMMs) to encode goal distributions for this environment, as illustrated in Fig. 7a. GMMs adequately capture the notion that the object is in the cabinet irrespective of the particular pose it comes to rest in inside the cabinet, including standing upright or toppled over on its side. We generate goal distributions by parametrically specifying a nominal GMM and generating samples from it. We then use the collision geometry of the bottle, table, and shelf and reject samples where the bottle is in collision with the table or shelf. We re-fit the GMM to the samples that are free of collision. We thereby achieve a goal distribution that has collision-free samples and satisfies the goal of “object in cabinet”. This procedure generalizes also to different cabinets, e.g. where shelves are differently spaced as shown in Fig. 7b.

A single-step plan for achieving the goal distribution is shown in Fig. 7b. In this case the shelf is high enough that the robot can execute a push lower on the bottle and slide the object into the cabinet. When the evenly-spaced shelves are more densely populated, as shown in Fig. 7b, it becomes infeasible to simply slide the upright bottle into the cabinet because it will collide with the shelf. Our multi-step skill planning approach finds a suitable plan that first executes a high-push to topple the bottle over onto its side, and then executes a low-push to slide the toppled object into the cabinet. We highlight the fact that the robot does not need to target a specific terminal object pose, nor does it have to precisely predict the outcome of executing the push skill. The robot leverages the goal distribution that encodes the semantic ambiguity of the goal, together with the propagated uncertainty of applying the its skills, to devise a coarse manipulation plan that achieves the desired outcome.

Our preliminary results suggest goal distributions and probabilistic skill effect predictions are a promising way forward for manipulation planning with more dynamic skills, and we are excited to see this idea taken further in future work. We discuss possible extensions to this application next in Sec. IX.

IX. DISCUSSION AND CONCLUSION

In this paper, we have argued that goal distributions are a more suitable goal representation than point-based goals for many problems in robotics. Goal distributions not only subsume traditional point-based and set-based goals but enable varied models of uncertainty the agent might have about its goal. We derived planning to goal distributions as an instance of planning as inference, thereby connecting our approach to the rich literature on planning as inference and enabling the use of a variety of solvers for planning to goal distributions. We additionally derived several cost reductions of our probabilistic planning formulation to common planning objectives in the literature. Our experiments showcased the flexibility of probability distributions as a goal representation, and the ease with which we can accommodate different models of goal uncertainty in our framework.

We believe there are many exciting avenues for future research in planning to goal distributions. One interesting direction is incorporating learning into our probabilistic planning framework. We see two key areas that will benefit

from learning. First, learning conditional generative models of goal distributions will provide a powerful and flexible goal representation for more complex environments and behaviors. This is also advocated for in [67], albeit for goal-conditioned policies in reinforcement learning. For example, learning mixture density networks [12] conditioned on a representation of the current environment configuration would enable learning scene-dependent multi-modal goal distributions. This could be paired with a multi-modal distribution in the planner as in Stein-variational methods [50] to enable parallelized planning to multiple goal regions simultaneously.

A second area we believe learning will benefit our probabilistic planning framework is in propagating the robot’s state uncertainty. The state spaces and dynamics functions utilized in our experiments were simple for demonstrative purposes, but more complex environments may require more advanced uncertainty propagation techniques to estimate the terminal state distribution well. For example, if the state space itself is a learned latent representation space, *normalizing flows* [45] may be an interesting technique to estimate how the latent state distribution transforms over the planning horizon.

In this paper, we only investigated cross-entropy and KL divergence as information-theoretic losses in our optimization. As we discussed in Sec. II, other losses are possible such as f -divergence [8, 28, 41] and Tsallis divergence [94]. Given the use of these broader classes of divergence in imitation learning [28, 41], reinforcement learning [8], and stochastic optimal control [94], we believe there are further opportunities in these related disciplines to utilize goal distributions beyond the planning framework we presented in this paper. We also foresee the utility of goal distributions in deterministic planning with uncertain goals, e.g. having Gaussian goal uncertainty and using Mahalanobis as a heuristic bias in sampling-based planning algorithms like RRT [51].

Our experiments in Sec. VIII-A demonstrated that minimizing the M-projection of cross-entropy is often necessary when we wish to model goals as distributions with finite support. We discussed in Sec. V-B4 how minimizing the M-projection of KL divergence and cross-entropy are equivalent for our optimizations since the entropy of the goal distribution is constant with respect to the decision variables. However, this is not always the case. Our experiments in Sec. VIII-C required the agent to maintain a belief of a moving target’s location which was updated at every timestep based on observations from a noisy sensor. The goal distribution was therefore dependent on the agent’s observations, which the agent has some control over. That is, the agent’s action determines in part what it will observe next, and the observation impacts what the goal distribution will be at the next timestep. Optimizing the M-projection in this case could therefore encourage the agent to reduce uncertainty about its goal and lead to exploratory behavior. However, the agent requires a model to predict what it will observe over its planning horizon, e.g. a maximum likelihood estimate in a POMDP setting [75]. This scenario is beyond the scope of the current paper but we believe this is an exciting application of our framework that deserves further investigation.

We showed in our results in Sec. VIII-B that our planning

approach could leverage a source of state uncertainty in the environment to more accurately match a goal state distribution. By embracing uncertainty both in the goal representation and how the agent predicts its state to transform over the planning horizon, our approach opens a wider array of behaviors that would typically be avoided by deterministic plans to point-based goals. For example, driving on mixed terrain [21] could be made more robust by modeling how the robot will behave driving over treacherous terrain like ice and mud. We believe leveraging sources of uncertainty in a controlled manner will open up more diverse robot behaviors. We looked at a simple example in the context of manipulation skill planning in Sec. VIII-E where predicting the distribution of poses an object might settle in after a manipulation enables utilizing more dynamic skills. We are excited to see this idea taken even further. For example, predicting the distribution of object poses resulting from a tossing robot [100] would enable planning to target locations outside the robot’s reachable workspace.

We believe goal distributions are a versatile and expressive goal representation for robots operating under uncertainty. The probabilistic planning framework we have presented in this article easily accommodates different goal distributions and probabilistic planning objectives. We foresee these techniques being particularly applicable to real-world robotics problems where state and goal uncertainty are inherent. We are excited by the prospect of embracing goal uncertainty explicitly in planning and control, especially when considering state or observation uncertainty. We anticipate many fruitful avenues of further research beyond what we have suggested here.

X. ACKNOWLEDGEMENT

This work is supported by DARPA under grant N66001-19-2-4035 and by NSF Award 2024778.

REFERENCES

- [1] List of probability distributions. https://en.wikipedia.org/wiki/List_of_probability_distributions, 2022. Accessed: 2022-01-27.
- [2] Hany Abdulsamad, Oleg Arenz, Jan Peters, and Gerhard Neumann. State-regularized policy search for linearized dynamical systems. In *Intl. Conf. on Automated Planning and Scheduling (ICAPS)*, 2017. URL http://www.ausy.tu-darmstadt.de/uploads/Site/EditPublication/Abdulsamad_ICAPS_2017.pdf.
- [3] Baris Akgun and Andrea Thomaz. Simultaneously learning actions and goals from demonstration. *Autonomous Robots*, 40(2):211–227, 2016.
- [4] Marcin Andrychowicz, Filip Wolski, Alex Ray, Jonas Schneider, Rachel Fong, Peter Welinder, Bob McGrew, Josh Tobin, OpenAI Pieter Abbeel, and Wojciech Zaremba. Hindsight experience replay. In *Advances in Neural Information Processing Systems (NeurIPS)*, pages 5048–5058, 2017.
- [5] Hagai Attias. Planning by probabilistic inference. In *International Workshop on Artificial Intelligence and Statistics*, pages 9–16. PMLR, 2003.
- [6] Adrien Baranes and Pierre-Yves Oudeyer. Active learning of inverse models with intrinsically motivated goal exploration in robots. *Robotics and Autonomous Systems*, 61(1):49–73, 2013.
- [7] Maxim A Batalin and Gaurav S Sukhatme. Coverage, exploration and deployment by a mobile robot and communication network. *Telecommunication Systems*, 26(2):181–196, 2004.
- [8] Boris Belousov and Jan Peters. f -divergence constrained policy improvement. 2018.
- [9] Mohak Bhardwaj, Balakumar Sundaralingam, Arsalan Mousavian, Nathan D Ratliff, Dieter Fox, Fabio Ramos, and Byron Boots. Storm: An integrated framework for fast joint-space model-predictive control for reactive manipulation. In *Conference on Robot Learning (CoRL)*, 2021.

- [10] Amit Bhatia, Matthew R. Maly, Lydia E. Kavraki, and Moshe Y Vardi. A multi-layered synergistic approach to motion planning with complex goals. *IEEE Robotics and Automation Magazine*, 18(3):55–64, 2011.
- [11] Christopher Bingham. An antipodally symmetric distribution on the sphere. *The Annals of Statistics*, pages 1201–1225, 1974.
- [12] Christopher M Bishop. Mixture density networks. Technical Report NCRG/94/004, Aston University, 1994.
- [13] Lars Blackmore, Masahiro Ono, Askar Bektassov, and Brian C. Williams. A Probabilistic Particle-Control Approximation of Chance-Constrained Stochastic Predictive Control. *IEEE Transactions on Robotics*, 2010.
- [14] Berk Calli, Arjun Singh, Aaron Walsman, Siddhartha Srinivasa, Pieter Abbeel, and Aaron M Dollar. The ycb object and model set: Towards common benchmarks for manipulation research. In *International Conference on Advanced Robotics (ICAR)*, pages 510–517. IEEE, 2015.
- [15] Salvatore Candido and Seth Hutchinson. Minimum uncertainty robot navigation using information-guided pomdp planning. In *IEEE Intl. Conf. on Robotics and Automation (ICRA)*, pages 6102–6108. IEEE, 2011.
- [16] Yevgen Chebotar, Mrinal Kalakrishnan, Ali Yahya, Adrian Li, Stefan Schaal, and Sergey Levine. Path integral guided policy search. In *IEEE Intl. Conf. on Robotics and Automation (ICRA)*, pages 3381–3388. IEEE, 2017.
- [17] David Coleman, Ioan Sucan, Sachin Chitta, and Nikolaus Correll. Reducing the barrier to entry of complex robotic software: a moveit! case study. *arxiv preprint*, 2014.
- [18] Adam Conkey and Tucker Hermans. Active learning of probabilistic movement primitives. In *2019 IEEE-RAS 19th International Conference on Humanoid Robots (Humanoids)*, pages 1–8. IEEE, 2019.
- [19] Fabio Cozman and Eric Krotkov. Truncated gaussians as tolerance sets. Technical report, Carnegie Mellon University, 1994.
- [20] Aidan Curtis, Xiaolin Fang, Leslie Pack Kaelbling, Tomás Lozano-Pérez, and Caelan Reed Garrett. Long-horizon manipulation of unknown objects via task and motion planning with estimated affordances. *arxiv preprint*, 2021.
- [21] Hendrik Dahlkamp, Adrian Kaehler, David Stavens, Sebastian Thrun, and Gary R Bradski. Self-supervised monocular road detection in desert terrain. In *Robotics: Science and Systems (RSS)*, volume 38, 2006.
- [22] Dawson-Haggerty et al. trimesh. URL <https://trimesh.org/>.
- [23] Marc Deisenroth and Carl E Rasmussen. Pilco: A model-based and data-efficient approach to policy search. In *Proceedings of the 28th International Conference on machine learning (ICML-11)*, pages 465–472, 2011.
- [24] Morteza Farrokhsiar and Homayoun Najjaran. Unscented model predictive control of chance constrained nonlinear systems. *Advanced Robotics*, 28(4):257–267, 2014.
- [25] Greg Foderaro, Silvia Ferrari, and M Zavlanos. A decentralized kernel density estimation approach to distributed robot path planning. In *Proceedings of the Neural Information Processing Systems Conference*, 2012.
- [26] Justin Fu, Avi Singh, Dibya Ghosh, Larry Yang, and Sergey Levine. Variational inverse control with events: A general framework for data-driven reward definition. *Advances in Neural Information Processing Systems (NeurIPS)*, 31, 2018.
- [27] Caelan Reed Garrett, Rohan Chitnis, Rachel Holladay, Beomjoon Kim, Tom Silver, Leslie Pack Kaelbling, and Tomás Lozano-Pérez. Integrated task and motion planning. *Annual Review of Control, Robotics, and Autonomous Systems*, 4:265–293, 2021.
- [28] Seyed Kamyar Seyed Ghasemipour, Richard Semel, and Shixiang Gu. A divergence minimization perspective on imitation learning methods. In *Conference on Robot Learning (CoRL)*, 2019.
- [29] Igor Gilitschenski, Gerhard Kurz, Simon J Julier, and Uwe D Hanebeck. Unscented orientation estimation based on the bingham distribution. *IEEE Transactions on Automatic Control*, 61(1):172–177, 2015.
- [30] Philip E Gill, Walter Murray, and Michael A Saunders. Snopt: An sqp algorithm for large-scale constrained optimization. *SIAM review*, 47(1):99–131, 2005.
- [31] Jared Glover and Leslie Pack Kaelbling. Tracking 3-d rotations with the quaternion bingham filter. 2013.
- [32] Jared Glover, Gary Bradski, and Radu Bogdan Rusu. Monte carlo pose estimation with quaternion kernels and the bingham distribution. In *Robotics: Science and Systems (RSS)*, volume 7, page 97, 2012.
- [33] Tuomas Haarnoja, Haoran Tang, Pieter Abbeel, and Sergey Levine. Reinforcement learning with deep energy-based policies. *arXiv preprint arXiv:1702.08165*, 2017.
- [34] Tuomas Haarnoja, Aurick Zhou, Pieter Abbeel, and Sergey Levine. Soft actor-critic: Off-policy maximum entropy deep reinforcement learning with a stochastic actor. *arXiv preprint arXiv:1801.01290*, 2018.
- [35] John R Hershey and Peder A Olsen. Approximating the kullback leibler divergence between gaussian mixture models. In *IEEE International Conference on Acoustics, Speech and Signal Processing*, volume 4, pages IV–317. IEEE, 2007.
- [36] Anthony Hotz and Robert E Skelton. Covariance control theory. *International Journal of Control*, 46(1):13–32, 1987.
- [37] Taylor A Howell, Chunjiang Fu, and Zachary Manchester. Direct policy optimization using deterministic sampling and collocation. *IEEE Robotics and Automation Letters*, 6(3):5324–5331, 2021.
- [38] Arun Iyer. Cross entropy of two normal distribution. <https://www.cse.iitb.ac.in/~aruniyer/kldivergencenormal.pdf>, 2022. Accessed: 2022-03-31.
- [39] Simon J Julier and Jeffrey K Uhlmann. New extension of the kalman filter to nonlinear systems. In *Signal processing, sensor fusion, and target recognition VI*, volume 3068, pages 182–193. International Society for Optics and Photonics, 1997.
- [40] Rudolph Emil Kalman. A new approach to linear filtering and prediction problems. *Transactions of the ASME-Journal of Basic Engineering*, 82(Series D):35–45, 1960.
- [41] Liyiming Ke, Sanjiban Choudhury, Matt Barnes, Wen Sun, Gilwoo Lee, and Siddhartha Srinivasa. Imitation Learning as f-Divergence Minimization. In *Workshop on the Algorithmic Foundations of Robotics*, 2020.
- [42] Alex Kendall and Yarin Gal. What uncertainties do we need in bayesian deep learning for computer vision? In *Advances in Neural Information Processing Systems (NeurIPS)*, pages 5580–5590, 2017.
- [43] Seungsu Kim, Ashwini Shukla, and Aude Billard. Catching objects in flight. *IEEE Transactions on Robotics*, 30(5):1049–1065, 2014.
- [44] Marin Kobilarov. Cross-entropy randomized motion planning. In *Robotics: Science and Systems (RSS)*, volume 7, pages 153–160, 2012.
- [45] Ivan Kobyzev, Simon Prince, and Marcus Brubaker. Normalizing flows: An introduction and review of current methods. *IEEE Transactions on Pattern Analysis and Machine Intelligence*, 2020.
- [46] Dorothea Koert, Susanne Trick, Marco Ewerton, Michael Lutter, and Jan Peters. Incremental learning of an open-ended collaborative skill library. *International Conference on Humanoid Robots (Humanoids)*, 17(01):2050001, 2020.
- [47] Yingyi Kuang, Abraham Itzhak Weinberg, George Vogiatzis, and Diego R Faria. Goal density-based hindsight experience prioritization for multi-goal robot manipulation reinforcement learning. In *IEEE International Conference on Robot and Human Interactive Communication (RO-MAN)*, 2020.
- [48] James Kuffner, Satoshi Kagami, Koichi Nishiwaki, Masayuki Inaba, and Hirochika Inoue. Online footprint planning for humanoid robots. In *IEEE Intl. Conf. on Robotics and Automation (ICRA)*, volume 1, pages 932–937. IEEE, 2003.
- [49] Miroslav Kárný. Towards fully probabilistic control design. *Automatica*, 32(12):1719–1722, 1996.
- [50] Alexander Lambert, Adam Fishman, Dieter Fox, Byron Boots, and Fabio Ramos. Stein Variational Model Predictive Control. In *Conference on Robot Learning (CoRL)*, 2020.
- [51] Steven M LaValle. Rapidly-exploring random trees: A new tool for path planning. 1998.
- [52] Steven M LaValle. *Planning Algorithms*. Cambridge university press, 2006.
- [53] Lisa Lee, Benjamin Eysenbach, Emilio Parisotto, Eric Xing, Sergey Levine, and Ruslan Salakhutdinov. Efficient Exploration via State Marginal Matching. In *ICLR Workshop*, 2018.
- [54] Sergey Levine. Reinforcement learning and control as probabilistic inference: Tutorial and review. *arxiv preprint*, 2018.
- [55] Thomas Lew, Apoorva Sharma, James Harrison, and Marco Pavone. Safe model-based meta-reinforcement learning: A sequential exploration-exploitation framework. *arxiv preprint*, 2020.
- [56] Jacky Liang, Mohit Sharma, Alex LaGrassa, Shivam Vats, Saumya Saxena, and Oliver Kroemer. Search-based task planning with learned skill effect models for lifelong robotic manipulation. In *IEEE Intl. Conf. on Robotics and Automation (ICRA)*, 2022.
- [57] Qingkai Lu, Kautilya Chenna, Balakumar Sundaralingam, and Tucker Hermans. Planning Multi-Fingered Grasps as Probabilistic Inference in a Learned Deep Network. In *International Symposium on Robotics Research (ISRR)*, 12 2017. URL <http://www.cs.utah.edu/~thermans/papers/lu-isrr2017-deep-multifinger-grasping.pdf>.
- [58] Qingkai Lu, Mark Van der Merwe, Balakumar Sundaralingam, and Tucker Hermans. Multi-Fingered Grasp Planning via Inference in Deep Neural Networks. *IEEE Robotics & Automation Magazine (Special*

- Issue on Deep Learning and Machine Learning in Robotics*), 27(2): 55–65, 2020. URL <https://arxiv.org/abs/2001.09242>.
- [59] Kevin M Lynch and Frank C Park. *Modern Robotics*. Cambridge University Press, 2017.
- [60] Guilherme Maeda, Marco Ewerton, Takayuki Osa, Baptiste Busch, and Jan Peters. Active incremental learning of robot movement primitives. In *Conference on Robot Learning (CoRL)*, pages 37–46. PMLR, 2017.
- [61] Guilherme J Maeda, Gerhard Neumann, Marco Ewerton, Rudolf Lioutikov, Oliver Kroemer, and Jan Peters. Probabilistic movement primitives for coordination of multiple human–robot collaborative tasks. *Autonomous Robots*, 41(3):593–612, 2017.
- [62] Prasanta Chandra Mahalanobis. On the generalized distance in statistics. National Institute of Science of India, 1936.
- [63] Andrew T Miller, Steffen Knoop, Henrik I Christensen, and Peter K Allen. Automatic grasp planning using shape primitives. In *IEEE Intl. Conf. on Robotics and Automation (ICRA)*, volume 2, pages 1824–1829. IEEE, 2003.
- [64] Mustafa Mukadam, Jing Dong, Xinyan Yan, Frank Dellaert, and Byron Boots. Continuous-time gaussian process motion planning via probabilistic inference. *The International Journal of Robotics Research*, 37(11):1319–1340, 2018.
- [65] Kevin P Murphy. *Machine learning: a probabilistic perspective*. MIT press, 2012.
- [66] Ashvin V Nair, Vitchyr Pong, Murtaza Dalal, Shikhar Bahl, Steven Lin, and Sergey Levine. Visual reinforcement learning with imagined goals. In *Advances in Neural Information Processing Systems (NeurIPS)*, pages 9191–9200, 2018.
- [67] Soroush Nasiriany, Vitchyr H Pong, Ashvin Nair, Alexander Khazatsky, Glen Berseth, and Sergey Levine. Disco rl: Distribution-conditioned reinforcement learning for general-purpose policies. In *IEEE Intl. Conf. on Robotics and Automation (ICRA)*, 2021.
- [68] Kazuhide Okamoto, Maxim Goldshtein, and Panagiotis Tsiotras. Optimal covariance control for stochastic systems under chance constraints. *IEEE Control Systems Letters*, 2(2):266–271, 2018.
- [69] Jia Pan, Sachin Chitta, and Dinesh Manocha. Fcl: A general purpose library for collision and proximity queries. In *IEEE Intl. Conf. on Robotics and Automation (ICRA)*, pages 3859–3866. IEEE, 2012.
- [70] Alexandros Paraschos, Christian Daniel, Jan Peters, and Gerhard Neumann. Using probabilistic movement primitives in robotics. *Autonomous Robots*, 42(3):529–551, 2018.
- [71] Valentin Peretroukhin, Matthew Giamou, David M Rosen, W Nicholas Greene, Nicholas Roy, and Jonathan Kelly. A smooth representation of belief over so (3) for deep rotation learning with uncertainty. In *Robotics: Science and Systems (RSS)*, 2020.
- [72] Jan Peters, Katharina Mülling, and Yasemin Altun. Relative entropy policy search. In *AAAI Conference on Artificial Intelligence (AAAI)*, volume 10, pages 1607–1612. Atlanta, 2010.
- [73] Joshua Pilipovsky and Panagiotis Tsiotras. Chance-constrained optimal covariance steering with iterative risk allocation. In *2021 American Control Conference (ACC)*, pages 2011–2016. IEEE, 2021.
- [74] Silviu Pitis, Harris Chan, Stephen Zhao, Bradley Stadie, and Jimmy Ba. Maximum entropy gain exploration for long horizon multi-goal reinforcement learning. *arxiv preprint*, 2020.
- [75] Robert Platt, Russ Tedrake, Leslie Kaelbling, and Tomas Lozano-Perez. Belief space planning assuming maximum likelihood observations. In *Robotics: Science and Systems (RSS)*, 2010.
- [76] Vitchyr H Pong, Murtaza Dalal, Steven Lin, Ashvin Nair, Shikhar Bahl, and Sergey Levine. Skew-fit: State-covering self-supervised reinforcement learning. *International Conference on Machine Learning (ICML)*, 2020.
- [77] Venkatesh G Rao and Dennis S Bernstein. Naive control of the double integrator. *IEEE Control Systems Magazine*, 21(5):86–97, 2001.
- [78] Konrad Rawlik, Marc Toussaint, and Sethu Vijayakumar. On Stochastic Optimal Control and Reinforcement Learning by Approximate Inference. In *Robotics: Science and Systems (RSS)*, 2012.
- [79] Zhizhou Ren, Kefan Dong, Yuan Zhou, Qiang Liu, and Jian Peng. Exploration via hindsight goal generation. In *Advances in Neural Information Processing Systems (NeurIPS)*, pages 13485–13496, 2019.
- [80] Jack Ridderhof, Kazuhide Okamoto, and Panagiotis Tsiotras. Chance constrained covariance control for linear stochastic systems with output feedback. In *2020 59th IEEE Conference on Decision and Control (CDC)*, pages 1758–1763. IEEE, 2020.
- [81] Keith Rudd, Greg Foderaro, Pingping Zhu, and Silvia Ferrari. A generalized reduced gradient method for the optimal control of very-large-scale robotic systems. *IEEE Transactions on Robotics*, 33(5): 1226–1232, 2017.
- [82] John Schulman, Sergey Levine, Pieter Abbeel, Michael Jordan, and Philipp Moritz. Trust region policy optimization. In *International Conference on Machine Learning (ICML)*, pages 1889–1897, 2015.
- [83] Anthony Simeonov, Yilun Du, Beomjoon Kim, Francois R Hogan, Joshua Tenenbaum, Pulkit Agrawal, and Alberto Rodriguez. A long horizon planning framework for manipulating rigid pointcloud objects. In *Conference on Robot Learning (CoRL)*, 2020.
- [84] Avi Singh, Larry Yang, Kristian Hartikainen, Chelsea Finn, and Sergey Levine. End-to-end robotic reinforcement learning without reward engineering. In *Robotics: Science and Systems (RSS)*, 2019.
- [85] Robert F Stengel. *Optimal control and estimation*. Courier Corporation, 1994.
- [86] Richard S Sutton and Andrew G Barto. *Reinforcement learning: An introduction*. MIT press, 2018.
- [87] Georges M Tallis. The moment generating function of the truncated multi-normal distribution. *Journal of the Royal Statistical Society: Series B (Methodological)*, 23(1):223–229, 1961.
- [88] Russ Tedrake and the Drake Development Team. Drake: Model-based design and verification for robotics, 2019. URL <https://drake.mit.edu>.
- [89] Sebastian Thrun, Wolfram Burgard, and Dieter Fox. *Probabilistic Robotics*. MIT press, 2005.
- [90] Marc Toussaint and Christian Goerick. A bayesian view on motor control and planning. In *From Motor Learning to Interaction Learning in Robots*, pages 227–252. Springer, Berlin, Heidelberg, 2010.
- [91] Jeffrey K Uhlmann. *Dynamic map building and localization: New theoretical foundations*. PhD thesis, University of Oxford, 1995.
- [92] Robert J Vanderbei. A case study in trajectory optimization: Putting on an uneven green. *SIAG/OPT Views-and-News*, 12(1):6–14, 2001.
- [93] Andreas Völz and Knut Graichen. Stochastic model predictive control of nonlinear continuous-time systems using the unscented transformation. In *European Control Conference*, pages 3365–3370. IEEE, 2015.
- [94] Ziyi Wang, Oswin So, Jason Gibson, Bogdan Vlahov, Manan Gandhi, Guan-Hong Liu, and Evangelos Theodorou. Variational Inference MPC using Tsallis Divergence. In *Robotics: Science and Systems (RSS)*, 2021.
- [95] Joe Watson and Jan Peters. Advancing trajectory optimization with approximate inference: Exploration, covariance control and adaptive risk. *arxiv preprint*, 2021.
- [96] Grady Williams, Andrew Aldrich, and Evangelos A Theodorou. Model predictive path integral control: From theory to parallel computation. *Journal of Guidance, Control, and Dynamics*, 40(2):344–357, 2017.
- [97] Grady Williams, Nolan Wagener, Brian Goldfain, Paul Drews, James M Rehg, Byron Boots, and Evangelos A Theodorou. Information theoretic mpc for model-based reinforcement learning. In *IEEE Intl. Conf. on Robotics and Automation (ICRA)*, pages 1714–1721. IEEE, 2017.
- [98] Fei Xia, Chengshu Li, Roberto Martín-Martín, Or Litany, Alexander Toshev, and Silvio Savarese. ReLMoGen: Leveraging motion generation in reinforcement learning for mobile manipulation. In *IEEE Intl. Conf. on Robotics and Automation (ICRA)*, 2021.
- [99] Ji Yin, Zhiyuan Zhang, Evangelos Theodorou, and Panagiotis Tsiotras. Improving model predictive path integral using covariance steering. *arxiv preprint*, 2021.
- [100] Andy Zeng, Shuran Song, Johnny Lee, Alberto Rodriguez, and Thomas Funkhouser. Tossingbot: Learning to throw arbitrary objects with residual physics. 2019.
- [101] Rui Zhao, Xudong Sun, and Volker Tresp. Maximum entropy-regularized multi-goal reinforcement learning. *arxiv preprint*, 2019.
- [102] Yi Zhou, Connelly Barnes, Jingwan Lu, Jimei Yang, and Hao Li. On the continuity of rotation representations in neural networks. pages 5745–5753, 2019.
- [103] Brian D Ziebart, Andrew L Maas, J Andrew Bagnell, and Anind K Dey. Maximum entropy inverse reinforcement learning. In *AAAI Conference on Artificial Intelligence (AAAI)*, volume 8, pages 1433–1438. Chicago, IL, USA, 2008.

APPENDIX A VARIATIONAL INFERENCE FOR PLANNING AS INFERENCE

We described at a high-level in Sec. V-A how variational inference techniques are often used to solve planning as inference problems. We now provide a more detailed derivation for the optimization objective in Eq. 9. This derivation is similar to that provided in [50] (cf. Appendix D in [50]).

Claim 1. *Consider the distribution of optimal trajectories $p(\tau \mid \mathcal{O}_\tau)$ and a proposal distribution $q(\tau) \in \mathcal{Q}$ from a family of distributions \mathcal{Q} . The objective*

$$q^* = \operatorname{argmin}_{q \in \mathcal{Q}} D_{\text{KL}}(q(\tau) \parallel p(\tau \mid \mathcal{O}_\tau)) \quad (40)$$

is equivalently solved by

$$q^* = \operatorname{argmin}_{q \in \mathcal{Q}} -\mathbb{E}_q[\log p(\mathcal{O}_\tau \mid \tau)] + D_{\text{KL}}(q(\tau) \parallel p(\tau)) \quad (41)$$

Proof: We have

$$q^* = \operatorname{argmin}_{q \in \mathcal{Q}} D_{\text{KL}}(q(\tau) \parallel p(\tau \mid \mathcal{O}_\tau)) \quad (42)$$

$$= \operatorname{argmin}_{q \in \mathcal{Q}} \int q(\tau) \log \frac{q(\tau)}{p(\tau \mid \mathcal{O}_\tau)} d\tau \quad (43)$$

$$= \operatorname{argmin}_{q \in \mathcal{Q}} \int q(\tau) \log \frac{q(\tau)}{p(\mathcal{O}_\tau \mid \tau)p(\tau)} d\tau \quad (44)$$

$$= \operatorname{argmin}_{q \in \mathcal{Q}} \int q(\tau) [\log q(\tau) - \log p(\mathcal{O}_\tau \mid \tau) - \log p(\tau)] d\tau \quad (45)$$

$$= \operatorname{argmin}_{q \in \mathcal{Q}} - \int q(\tau) \log p(\mathcal{O}_\tau \mid \tau) d\tau + \int q(\tau) [\log q(\tau) - \log p(\tau)] d\tau \quad (46)$$

$$= \operatorname{argmin}_{q \in \mathcal{Q}} - \int q(\tau) \log p(\mathcal{O}_\tau \mid \tau) d\tau + \int q(\tau) \log \frac{q(\tau)}{p(\tau)} d\tau \quad (47)$$

$$= \operatorname{argmin}_{q \in \mathcal{Q}} -\mathbb{E}_q[\log p(\mathcal{O}_\tau \mid \tau)] + D_{\text{KL}}(q(\tau) \parallel p(\tau)) \quad (48)$$

■

This establishes Eq. 9 in V-A. Note the KL term in Eq. 48 regularizes the trajectory distribution $q(\tau)$ to a prior distribution $p(\tau)$. As such, we denote the prior distribution by $p_0(\tau)$ in Eq. 9. This objective is equivalent to maximizing the *evidence lower bound (ELBO)* expressed by

$$q^* = \operatorname{argmax}_{q \in \mathcal{Q}} \mathbb{E}_q[\log p(\mathcal{O}_\tau \mid \tau)] - D_{\text{KL}}(q(\tau) \parallel p_0(\tau)) \quad (49)$$

which is a common variational objective in machine learning more generally.

APPENDIX B ALTERNATIVE DERIVATION FOR GOAL DISTRIBUTIONS IN PLANNING AS INFERENCE

We now present an alternative derivation for our results in Sec. V-B. We re-derive the planning as inference and stochastic optimality duality from [78] taking special care to introduce the optimal goal distribution for the terminal cost to fit our needs.

In planning as inference we wish to minimize the following objective

$$q^* = \operatorname{argmin}_q D_{\text{KL}}(q(\tau) \parallel p(\tau \mid \mathcal{O} = 1)) \quad (50)$$

where the variational q has the form:

$$q(\tau) = q(\mathbf{x}_0) \prod_{t=0}^{T-1} q(\mathbf{x}_{t+1} \mid \mathbf{x}_t, \mathbf{u}_t) \pi_q(\mathbf{u}_t \mid \mathbf{x}_t) \quad (51)$$

and the optimal trajectory distribution has the form

$$p(\tau \mid \mathcal{O} = 1) \propto p(\tau, \mathcal{O} = 1) = p(\mathbf{x}_0) p(\mathcal{O}_T = 1 \mid \mathbf{x}_T) \prod_{t=0}^{T-1} p(\mathcal{O} = 1 \mid \mathbf{x}_t, \mathbf{u}_t) p(\mathbf{x}_{t+1} \mid \mathbf{x}_t, \mathbf{u}_t) \pi_0(\mathbf{u}_t \mid \mathbf{x}_t) \quad (52)$$

We now plug the trajectory distribution definitions into the KL objective and expanding terms.

$$D_{\text{KL}}(q(\tau) \parallel p(\tau \mid \mathcal{O} = 1)) = \mathbb{E}_{q(\tau)} \left[\ln \frac{q(\mathbf{x}_0) \prod_{t=0}^{T-1} q(\mathbf{x}_{t+1} | \mathbf{x}_t, \mathbf{u}_t) \pi_q(\mathbf{u}_t | \mathbf{x}_t)}{p(\mathbf{x}_0) p(\mathcal{O} = 1 | \mathbf{x}_T) \prod_{t=0}^{T-1} p(\mathcal{O} = 1 | \mathbf{x}_t, \mathbf{u}_t) p(\mathbf{x}_{t+1} | \mathbf{x}_t, \mathbf{u}_t) \pi_0(\mathbf{u}_t | \mathbf{x}_t)} \right] \quad (53)$$

$$= \mathbb{E}_{q(\tau)} \left[\ln \left[q(\mathbf{x}_0) \prod_{t=0}^{T-1} q(\mathbf{x}_{t+1} | \mathbf{x}_t, \mathbf{u}_t) \pi_q(\mathbf{u}_t | \mathbf{x}_t) \right] - \ln \left[p(\mathbf{x}_0) p(\mathcal{O} = 1 | \mathbf{x}_T) \prod_{t=0}^{T-1} p(\mathcal{O} = 1 | \mathbf{x}_t, \mathbf{u}_t) p(\mathbf{x}_{t+1} | \mathbf{x}_t, \mathbf{u}_t) \pi_0(\mathbf{u}_t | \mathbf{x}_t) \right] \right] \quad (54)$$

$$= \mathbb{E}_{q(\tau)} [\ln q(\mathbf{x}_0) - \ln p(\mathbf{x}_0) + \sum_{t=0}^{T-1} \ln q(\mathbf{x}_{t+1} | \mathbf{x}_t, \mathbf{u}_t) - \sum_{t=0}^{T-1} \ln p(\mathbf{x}_{t+1} | \mathbf{x}_t, \mathbf{u}_t) \quad (55)$$

$$+ \sum_{t=0}^{T-1} \ln \pi_q(\mathbf{u}_t | \mathbf{x}_t) - \ln p(\mathcal{O} = 1 | \mathbf{x}_T) - \sum_{t=0}^{T-1} \ln p(\mathcal{O} = 1 | \mathbf{x}_t, \mathbf{u}_t) - \sum_{t=0}^{T-1} \ln \pi_0(\mathbf{u}_t | \mathbf{x}_t)] \quad (56)$$

We make the common assumption [54] that we have the correct estimate of the initial distribution $p(\mathbf{x}_0) = q(\mathbf{x}_0)$ from our state estimation process as well as the correct dynamics model $q(\mathbf{x}_{t+1} | \mathbf{x}_t, \mathbf{u}_t) = p(\mathbf{x}_{t+1} | \mathbf{x}_t, \mathbf{u}_t)$. Then the objective simplifies to

$$D_{\text{KL}}(q(\tau) \parallel p(\tau \mid \mathcal{O} = 1)) = \mathbb{E}_{q(\tau)} \left[\sum_{t=0}^{T-1} \ln \pi_q(\mathbf{u}_t | \mathbf{x}_t) - \ln p(\mathcal{O} = 1 | \mathbf{x}_T) - \sum_{t=0}^{T-1} \ln p(\mathcal{O} = 1 | \mathbf{x}_t, \mathbf{u}_t) - \sum_{t=0}^{T-1} \ln \pi_0(\mathbf{u}_t | \mathbf{x}_t) \right] \quad (57)$$

If we further assume that the policy is deterministic $\pi_q(\mathbf{u}_t | \mathbf{x}_t) = \delta_{\mathbf{u}_t = \phi(\mathbf{x}_t)}$, we are able to integrate the term out:

$$D_{\text{KL}}(q(\tau) \parallel p(\tau \mid \mathcal{O} = 1)) = \mathbb{E}_{q(\tau)} \left[-\ln p(\mathcal{O} = 1 | \mathbf{x}_T) - \sum_{t=0}^{T-1} \ln p(\mathcal{O} = 1 | \mathbf{x}_t, \mathbf{u}_t) - \sum_{t=0}^{T-1} \ln \pi_0(\mathbf{u}_t | \mathbf{x}_t) \right] \quad (58)$$

We now assert our optimality distributions, namely that the terminal state reaches the estimated goal, $p(\mathcal{O} = 1 | \mathbf{x}_T) = p_g(\mathbf{x}_T)$ and our non-terminal optimality conditions are exponentiated negative cost (i.e. reward), $p(\mathcal{O} = 1 | \mathbf{x}_t, \mathbf{u}_t) = \exp\{-\alpha c_t(\mathbf{x}_t, \mathbf{u}_t)\}$. We get the objective of

$$D_{\text{KL}}(q(\tau) \parallel p(\tau \mid \mathcal{O} = 1)) = \mathbb{E}_{q(\tau)} \left[-\ln p_g(\mathbf{x}_T) + \sum_{t=0}^{T-1} -\alpha c_t(\mathbf{x}_t, \mathbf{u}_t) - \sum_{t=0}^{T-1} \ln \pi_0(\mathbf{u}_t | \mathbf{x}_t) \right] \quad (59)$$

Which shows us that we wish to minimize the sum of the expected negative log likelihood of reaching the goal, the expected running costs (scaled by α) as well as a term penalizing low entropy in the prior policy. However, if we assume a uniform prior policy $\pi_0(\mathbf{u}_t | \mathbf{x}_t) = \mathbb{U}(\mathbf{u}_t | \mathcal{U})$ then we obtain the simpler form

$$\argmin_{\pi} D_{\text{KL}}(q(\tau) \parallel p(\tau \mid \mathcal{O} = 1)) = \argmin_{\pi} \mathbb{E}_{q(\tau)} \left[-\ln p_g(\mathbf{x}_T) + \sum_{t=0}^{T-1} -\alpha c_t(\mathbf{x}_t, \mathbf{u}_t) \right] \quad (60)$$

Which is equivalent to maximizing the expected probability of reaching the goal, times the Boltzman distribution over costs:

$$\min \mathbb{E}_{q(\tau)} \left[-\ln p_g(\mathbf{x}_T) + \sum_{t=0}^{T-1} -\alpha c_t(\mathbf{x}_t, \mathbf{u}_t) \right] \equiv \max \mathbb{E}_{q(\tau)} \left[p_g(\mathbf{x}_T) \prod_{t=0}^{T-1} \exp\{-\alpha c_t(\mathbf{x}_t, \mathbf{u}_t)\} \right] \quad (61)$$

Let $\lambda = \frac{1}{\alpha}$, then

$$\pi^* = \argmin_{\pi} \mathbb{E}_{q(\tau)} \left[-\ln p_g(\mathbf{x}_T) + \sum_{t=0}^{T-1} -\alpha c_t(\mathbf{x}_t, \mathbf{u}_t) \right] \quad (62)$$

$$= \argmin_{\pi} \mathbb{E}_{q(\tau)} \left[-\ln p_g(\mathbf{x}_T) + \sum_{t=0}^{T-1} -\alpha c_t(\mathbf{x}_t, \mathbf{u}_t) \right] \cdot \lambda \quad (63)$$

$$= \argmin_{\pi} \mathbb{E}_{q(\tau)} \left[-\lambda \ln p_g(\mathbf{x}_T) + \sum_{t=0}^{T-1} -c_t(\mathbf{x}_t, \mathbf{u}_t) \right] \quad (64)$$

which we can interpret as a Lagrange multiplier on the terminal cost term, enforcing an inequality constraint that $E_{q(\tau)}[p_g(\mathbf{x}_T)] > (1 - \epsilon)$ and if this is not met we can update the dual parameter λ and re-solve the unconstrained optimization problem.

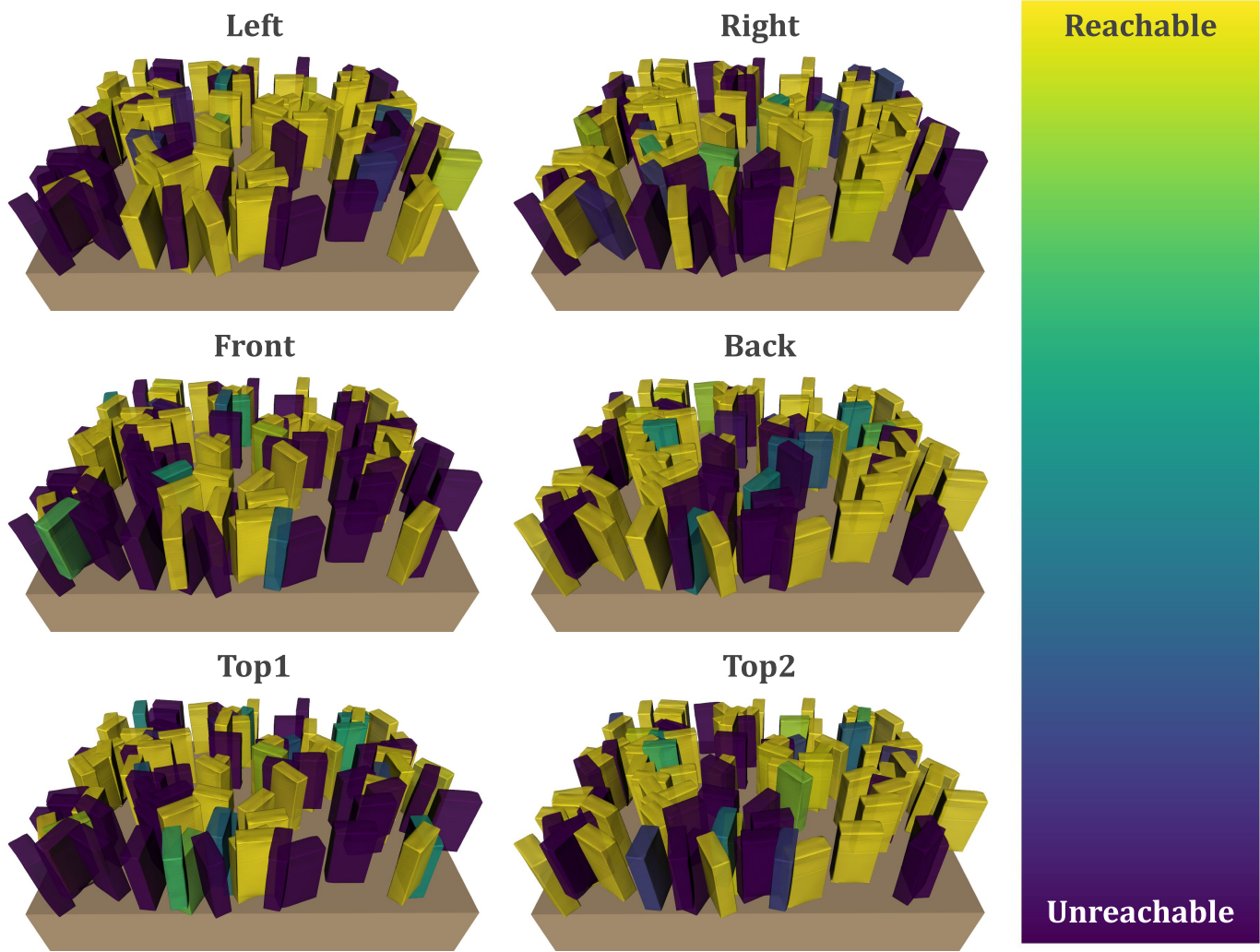


Fig. 8: Comparison of the reachability of the different distribution components of the pose mixture model used in our arm-reaching experiments in Sec. VIII-D. Each sub-figure visualizes the object mesh in the same 100 random poses on the table where the mesh color indicates whether the component was reachable (yellow/green) or unreachable (blue/purple) for that object pose. Reachability is computed as described in Sec. VIII-D.

APPENDIX C

ARM REACHING – ADDITIONAL DETAILS

We provide some additional visualizations (Fig. 8) for our arm-reaching experiments from Sec. VIII-D to offer more intuition for the reachability of the different components in the pose mixture model we defined. As a reminder, reachability of a component is determined by computing inverse kinematics for 100 samples and counting how many samples were reachable. A component is deemed reachable if at least 50 of the samples are reachable.

We found that some components are reachable in certain object poses and not others. Additionally, for every object pose, there was typically at least one component that was unreachable. Of the 100 object poses, there were only 5 instances where all components were reachable. 88 of the 100 poses had at least one component with zero reachable samples.

We visualize the component reachability in Fig. 8. Every sub-figure shows the object mesh in the same 100 uniformly random poses we used in our experiments in Sec. VIII-D, where the color of the mesh indicates the reachability of the associated component. Each sub-figure visualizes reachability for a different component. The color gradient shown in the right side of the figure determines the interpretation of the mesh colors, where yellow means the component is highly-reachable, purple means the component is highly-unreachable, and green and blue are on the spectrum in between.

Note that there are far more instances where the components are nearly completely reachable or completely unreachable in comparison to instances that fall in the middle of that spectrum. This aligns well with our intuition – if one pose is reachable, it’s likely that small perturbations of that pose will also be reachable. However, there are instances where a pose is perhaps reachable but close to the edge of the reachable workspace, or the robot may be near a joint limit. In these instances, small perturbations to a reachable pose may lead to unreachable samples.

APPENDIX D SOLVER DETAILS

We utilized a variety of solvers in our experiments in Sec. VIII including gradient-based and sampling-based solvers. We will here describe in more details the particular solvers and hyperparameters we used. We emphasize that we did not expend undue effort optimizing hyperparameters and it is likely different solvers and hyperparameters will have better performance on our problems.

A. Dubins Planar Navigation Environment

We used a gradient-based solver for the planar navigation environment in Sec. VIII-A. We formulated our problem as a constrained optimization problem in Drake [88] and used the SNOPT [30] solver. We used the following hyperparameters and parameter settings:

Parameter	Value	Description
I	200	Maximum number of iterations to run solver
T	45	Planning horizon
dt	0.3	Timestep
ω_t	0.002	Variance for dynamics noise (isotropic Gaussian)
Σ_0	0.02	Initial state covariance (isotropic Gaussian)
β	2	Parameter to unscented transform governing sigma point dispersion

We used the default values provided by the Drake interface to SNOPT for all SNOPT hyperparameters not mentioned in the table.

B. Ball-Rolling Environment

We used the *cross-entropy method (CEM)* [44] for our solver for the ball-rolling problem in Sec. VIII-B. CEM is a sampling-based solver that generates solution samples from a Gaussian distribution, evaluates the cost of each sample, and re-fits the distribution for the next iteration using the samples with the lowest cost (a.k.a. the *elite set*). The CEM update rule has been derived from a planning as inference framework assuming an optimality likelihood with thresholded utility [50].

We note that in principle the gradient solver from Appendix D-A could be used for this problem, but in practice it was highly sensitive to the initial solution and would frequently get stuck in local optima. In contrast, CEM found solutions very quickly (within approximately 5-10 iterations) and was not as susceptible to local optima. We used the following parameter settings:

Parameter	Value	Description
I	50	Maximum number of iterations to run CEM
N	500	Number of samples generated in each CEM iteration
K	20	Number of elite samples to re-fit CEM sampling distribution to
σ_0^2	0.8	Initial covariance for the CEM sampling distribution (isotropic Gaussian)
H	100	Planning horizon
dt	0.3	Timestep
ω_t	0.0001	Nominal variance for dynamics noise (isotropic Gaussian)
ω'_t	0.008	Additional noise from amplifier (isotropic Gaussian)
β	2	Parameter to unscented transform governing sigma point dispersion

Note the planning horizon for this environment is modeling the passive dynamics of the rolling ball, since controls are only applied at the initial timestep to initiate the motion of the ball.

C. Target Intercept Environment

We use *model predictive path integral control (MPPI)* [96] for our dynamic goal experiments in Sec. VIII-C. MPPI is a sampling-based solver that iteratively updates a Gaussian distribution of solutions by generating noisy perturbations of the current mean solution at each iteration. A weighted average of the samples is computed to determine the new mean solution, where higher cost samples contribute less to the update. This procedure is carried out in a model predictive control (MPC) scheme such that a plan for a small horizon is generated at every iteration, the first action of that plan is executed, and the agent re-plans at the next iteration. This procedure is widely used in robotics due to its computational simplicity, ease of parallelization [9], and applicability to complex problems even when the cost is non-differentiable. See [96] for a more detailed and formal presentation of MPPI.

We used the following parameter settings:

Parameter	Value	Description
I	70	Number of iterations to run MPC
N	100	Number of samples generated in each MPPI iteration
σ_0^2	0.02	Initial variance for the MPPI sampling distribution (isotropic Gaussian)
σ_N^2	0.002	Terminal variance for the MPPI sampling distribution (isotropic Gaussian)
H_{\max}	25	Maximum planning horizon
H_{\min}	3	Minimum planning horizon

Note we employ a couple of strategies to get better results:

- 1) We reduce the MPPI variance from σ_0^2 to σ_N^2 in even steps over the number of MPPI iterations I . We found this strategy to produce better results since it can find more refined solutions as the number of MPPI iterations increases.
- 2) We dynamically adapt the planning horizon to start at a maximum of H_{\max} and reduce to a minimum of H_{\min} based on how far the agent is from the target. In order to adapt this value based only on information available to the agent, we use the KL divergence between the agent’s state distribution and the projected belief distribution as a measure of proximity so that as the agent gets closer to the target, it uses a shorter planning horizon.

D. Arm-Reaching Environment

We use MPPI as our solver for the arm reaching environment from our experiments in Sec. VIII-D. We note again that in principle the gradient-based solver could in principle be used for this environment. However, the solver required a good initial solution in order to find a valid plan, and the initial solutions ended up over-biasing the solver to particular components to reach to. We found the sampling scheme of MPPI to produce the least biased results. Note that we are not using MPPI in an MPC setting as we did in Appendix D-C, but instead just using the MPPI sampling and update scheme to efficiently find solutions for the full planning horizon. We used the following settings:

Parameter	Value	Description
I	30	Maximum number of iterations to run MPPI
N	500	Number of samples generated in each MPPI iteration
σ_0^2	0.002	Initial variance for the MPPI sampling distribution (isotropic Gaussian)
σ_N^2	0.0001	Terminal variance for the MPPI sampling distribution (isotropic Gaussian)
H	10	Planning horizon

APPENDIX E SKILL PLANNING – ADDITIONAL DETAILS

In this appendix, we provide additional details on our experiments from Sec. VIII-E regarding applying our probabilistic planning framework to the domain of skill planning.

A. Generating Goal Distributions

While goal distributions are a more expressive goal representation than single points, it may be more of a burden to acquire a meaningful goal distribution in certain contexts. In this section, we describe how we generated the Gaussian mixture model goal distribution we used in Sec. VIII-E to capture the semantic goal of “object on a shelf of bookcase”, shown in Fig. 9. We assume object and environment meshes are given.

We perform the following steps to generate a goal GMM:

- 1) **Compute stable object poses:** We compute stable poses (also known as *support surfaces*) for the object to be placed on the shelf. We utilize Trimesh [22] for this purpose, which computes stable poses by evaluating the probability of landing in random poses when dropped onto a table. The output is a small number of stable poses the object can be on a planar surface. In the case of the cleaner bottle we utilize in our experiments, it computed three stable poses (shown in Fig. 9a): one upright, one on the front flat side, and one on the rear flat side. We translate these stable poses to the center of the shelf surface for which we’re generating a goal distribution for.
- 2) **Generate random perturbations of stable poses:** We generate random planar pose perturbations from a zero-mean Gaussian distribution with a small, manually set variance. We compose these perturbations with each stable pose to produce a set of pose samples resting on the shelf surface (Fig. 9b).
- 3) **Filter out samples in collision:** Many of the samples may collide with the walls of the shelf if the variance is set high enough. We reject these samples using the Trimesh [22] interface to the Flexible Collision Library (FCL) [69]. Note we take the convex hull of the object mesh to speed up collision checking. Samples in collision are shown in Fig. 9c.
- 4) **Filter out samples not contained by the shelf:** Some samples may have been generated outside the support surface of the shelf, and even out of the boundary of the shelf entirely. We filter these samples by checking whether the object mesh is contained within the bounding box of the shelf. Fig. 9e shows the samples not contained within the bookcase,

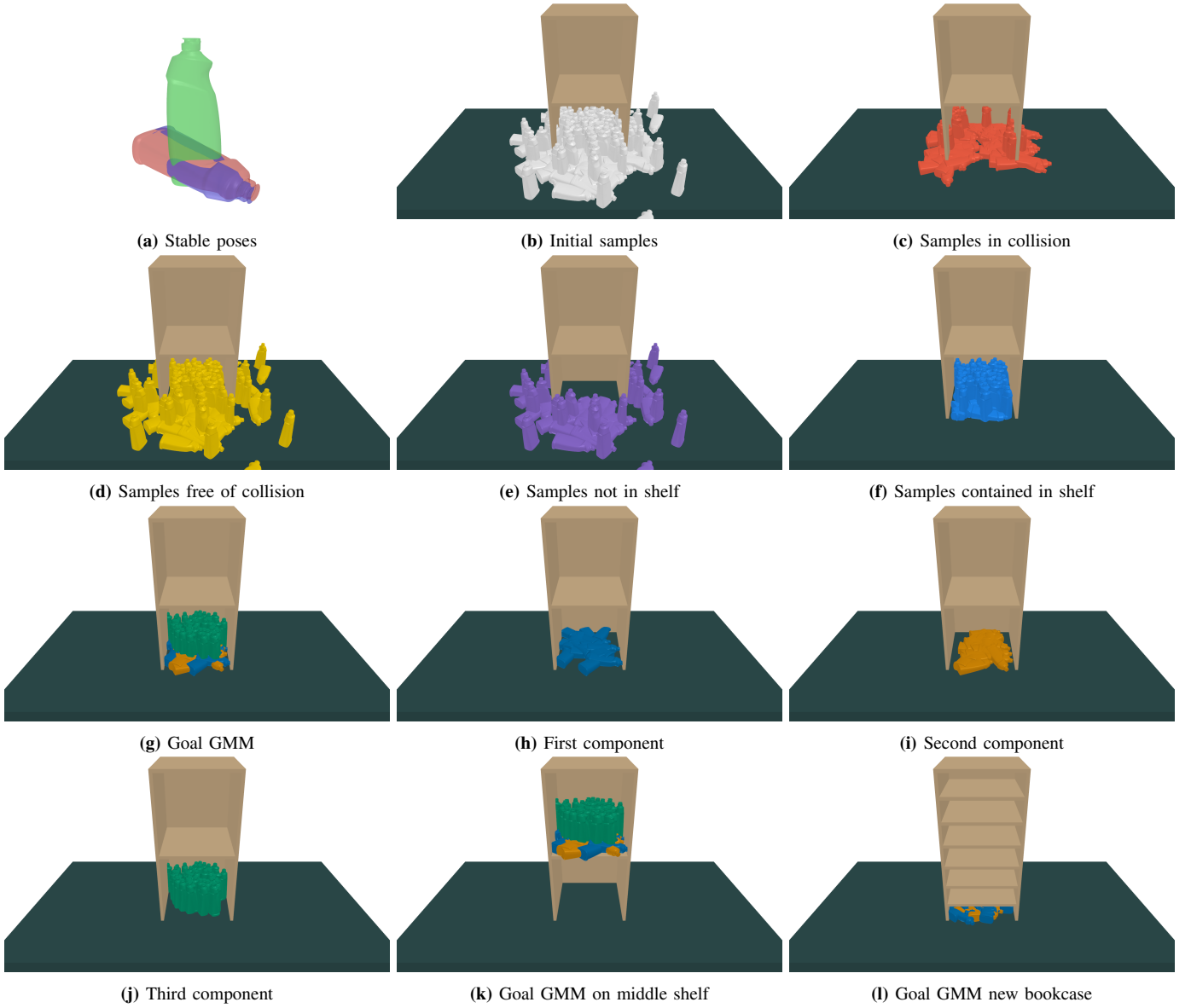


Fig. 9: Example goal distribution generation process for the goal of “cleaner bottle on shelf” of a bookcase. (a) Stable poses of the object on a support surface. (b) Pose samples generated from Gaussian-distributed planar perturbations of the stable poses. (c) Pose samples that place the object in collision with the shelf. (d) Samples free of collision with the environment. (e) Samples not contained within the bounding box of the shelf. (f) Samples contained within the shelf. (g) The resulting goal GMM fit to the collection of valid samples. (h) The first GMM component, with the bottle laying on its front side. (i) The second GMM component, with the bottle laying on its back side. (j) The third GMM component, with the bottle standing upright. (k) The goal GMM generated on the middle shelf of the bookcase. (l) Goal GMM generated for a different bookcase with lower shelves, which disallows samples with the bottle upright.

and Fig. 9f shows contained samples. Note this step might be used in lieu of (3) since containment in the bounding box will likely filter the samples in collision. However, we include both steps for generality since the collision checking may still be needed if, e.g., there are other objects on the shelf.

- 5) **Fit a parametric distribution to the samples:** We fit a Gaussian mixture model to the samples. We can conveniently set the number of GMM components to be the number of stable poses computed in (1). In this case we get the resulting 3-component GMM visualized in Fig. 9g where the individual components are shown in Fig. 9h, Fig. 9i, and Fig. 9j.

This procedure can be performed for any of the shelves in the bookcase once the height of the shelf support surface is known. We generate the goal GMM on the middle shelf of the bookcase in Fig. 9k. Due to the collision-aware sampling, we can also generate the goal distribution when shelves are more closely spaced apart, as shown in Fig. 9l. The shorter shelves require the bottle to lay on one of its flat sides and prevent the bottle from sitting upright. Our generation process automatically handles this case when in-collision samples are filtered out in step (3).

This process is also not limited to this environment, and each phase may be relaxed to achieve the desired goal distribution.

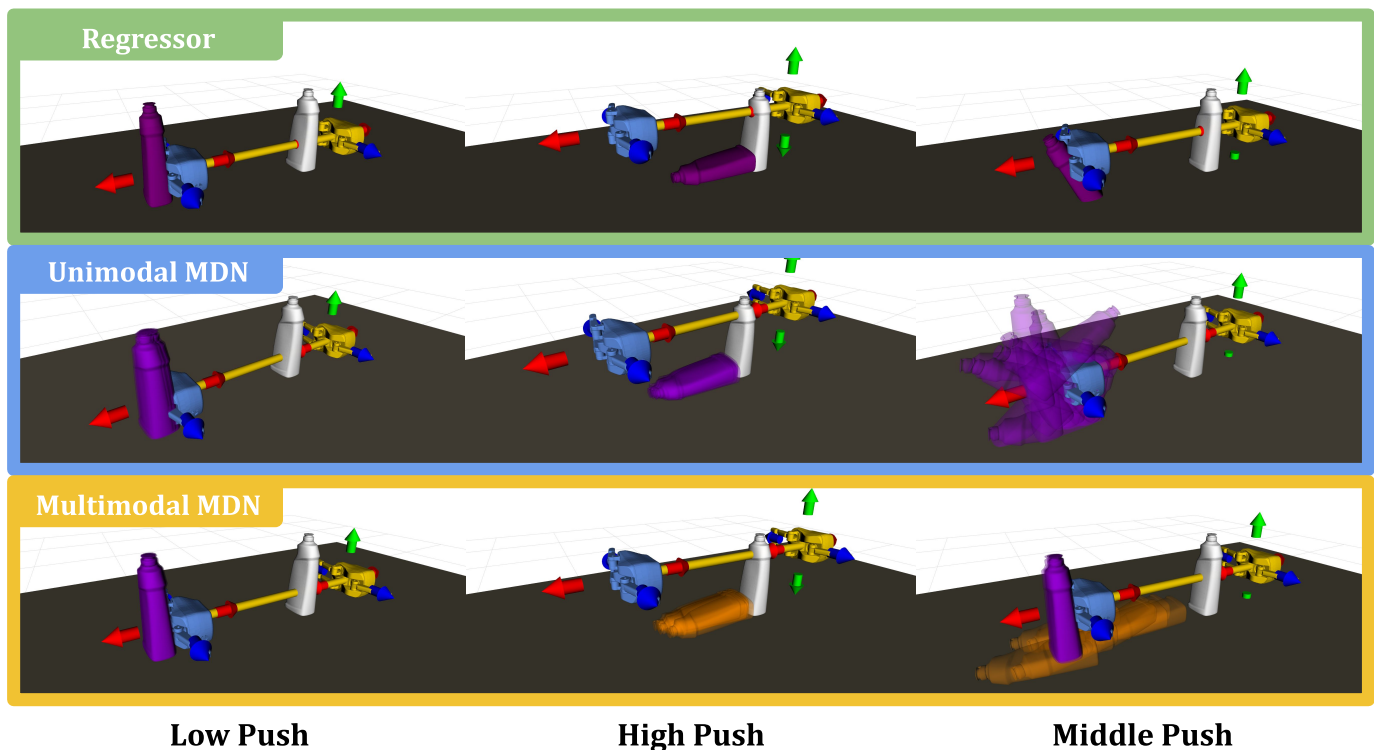


Fig. 10: Qualitative comparisons of point-based (regressor), unimodal (1-component MDN), and multimodal (2-component MDN) outcome predictions for the push skill pushing at low, high, and middle heights. For low-pushes (**left column**) and high-pushes (**middle column**) all three models give reasonable predictions of the object remaining upright and toppled, respectively. However, for middle-pushes (**right column**), only the multimodal MDN (**bottom row**) gives plausible predictions with one mode for the object remaining upright and a second mode with the object toppled. In contrast, the point-based regressor (**top row**) predicts the object in a half-toppled state, and the unimodal predictor (**middle row**) predicts a distribution with samples dispersed in the air and in collision with the end-effector.

We note that for more complex scenarios, collision and containment checks may not be sufficient. For example, if we had the goal of “object in bin”, the object in that case may not be limited to resting only on its support surfaces. In this case, we might want to leverage a physics simulator to spawn the object randomly above the bin and let the object fall into the bin. Using physics-informed constraints and heuristics to filter samples enables acquiring goal distributions that are meaningful for manipulation without the burden of having to manually specify associated uncertainty parameters for a particular goal.

B. Data Collection

We use the NVIDIA Isaac Gym simulator for all data collection for our skills from Sec. VIII-E. We developed engineered, motion-planned behaviors³ using MoveIt [17] to support autonomous collection. The Isaac Gym simulator enables several environments (we used 16) to run in parallel on a single machine. This together with our engineered behaviors enables large scale data collection. We were able to collect 10,000 instances of a push skill in approximately 12 hours on a Linux machine with Ubuntu 20.04, an Intel Core i7 processor, and an NVIDIA RTX2070 GPU.

C. Point-Based Versus Unimodal Versus Multimodal Predictions

We compare different choices for the skill effect model outputs. In Sec. VIII-E we indicated we desire multimodal predictions to capture different manipulation modes the object might end up in. We provide some qualitative results here to support this idea, shown in Fig. 10.

Our learned models⁴ were developed in PyTorch. Our MDN model consisted of two hidden layers each of size 256 with ReLU activations. Since we predict distributions over (delta) object poses, standard MDNs [12] are insufficient since the inputs and predictions must satisfy the constraints of $SE(3)$ rigid body transformations. Common parameterizations of rotations like quaternions and Euler angles introduce discontinuities that are difficult for neural networks to learn [102]. We address this problem by utilizing the learned 6D representation described in [102] that uses a Gram-Schmidt process to ensure orthogonalization. This provides us with a continuous representation for orientations to learn skill effect models over object

³Code for our engineered behaviors: https://bitbucket.org/robot-learning/l14ma_isaacgym

⁴Code for our learned models: https://bitbucket.org/robot-learning/multisensory_learning

poses. The point-based models also have two hidden layers of size 256 with ReLU activations, and differ only in the output – instead of predicting the parameters of a GMM they predict only a single point estimate

We train three different skill effect models for pushing the cleaner bottle from the YCB dataset [14]. All three models receive the same input, which is a single point-based estimate of the initial object pose, as well as the parameters for the push skill, which consist of the initial and terminal end-effector poses in the object frame. The models differ only in the training loss and class of predicted output. The models each output the predicted change in object pose from its initial pose, where they predict either a point estimate or a distribution over poses. We then compare model predictions for different push heights where the object should remain upright for low-pushes, topple for high-pushes, and there should be some uncertainty about whether it topples or remains upright for middle pushes.

We train a point-based regressor (top row of Fig. 10) that predicts the terminal pose of the object upon executing the push skill. This model is trained with a regression loss using the ground truth terminal pose as the target, where the loss is computed as the sum of the position and rotation error between the predicted and ground truth object pose

$$\mathcal{L}_{\text{reg}} = \|\mathbf{p} - \hat{\mathbf{p}}\|_2^2 + \theta_R \quad (65)$$

where position error is the L2-norm between the predicted position $\hat{\mathbf{p}}$ and ground truth position \mathbf{p} , and θ_R is the L2-norm of the matrix-logarithm error [59] between the predicted orientation $\hat{\mathbf{R}}$ and ground truth orientation \mathbf{R} . We see that a low push (top row, left column) and a high push (top row, middle column) produce reasonable predictions of the object upright and toppled, respectively. However, for a middle push, the model tends to predict the object is suspended halfway between upright and toppled (top row, right column). We also train a unimodal predictor, which is a single-component MDN (middle row, right column) trained with the MDN loss defined as

$$\mathcal{L}_{\text{MDN}}(\boldsymbol{\xi}) = \frac{1}{|\mathcal{D}|} \sum_{(\boldsymbol{\omega}_t, \mathbf{x}_{t+1}, \boldsymbol{\theta}) \in \mathcal{D}} -\log p(\mathbf{x}_{t+1} | \boldsymbol{\omega}_t, \boldsymbol{\theta}, \{\alpha_{t+1}^i, \boldsymbol{\mu}_{t+1}^i, \boldsymbol{\Sigma}_{t+1}^i\}_{i=1}^M) \quad (66)$$

where \mathcal{D} is a training dataset of state transitions and skill parameters. Similar to the regressor, predictions are reasonable for low and high pushes having Gaussian predictions with low variance of the object upright and toppled, respectively. However, the middle pushes where there is ambiguity about it being toppled or upright result in a Gaussian prediction with samples dispersed in the air and in collision with the end-effector and the table. In contrast to the regressor and the unimodal MDN, a 2-component MDN (bottom row, right column) captures both possibilities of the middle push, one component with the object upright and another with it toppled.

While it may seem innocuous that the point-based and unimodal models produce bad predictions on occasion, we find that even seemingly rare bad predictions are easily exploited by the planner. Our multimodal predictions mitigate some of these exploits. We discuss additional ways in which poor model predictions were exploited by the planner, and how we remedied those scenarios in the next section.

D. Fixing Erroneous Model Predictions Exploited by Planner

Ideally we can learn models only from instances of the robot executing skills successfully in order to capture correct outcome predictions for the object. However, unless the planner is restricted to optimizing actions only seen in the training data, it is wonderfully proficient at finding actions outside the training data where model predictions are nonsensical, and exploiting them. We provide examples we encountered in Fig. 11. In these examples, the robot was tasked to simply push the bottle from its initial pose (blue mesh) to a target pose 40cm away. The orange meshes in Fig. 11a show a correct prediction and the intended push for the planner to find.

However, because the training data contained no instances of the end-effector in a penetrating collision with the object (a physical impossibility), the planner exploits that condition as shown in Fig. 11b and believes it can achieve the target pose by penetrating the object and executing a long push past the target pose. In order to remedy this, we incorporate a collision cost as an auxiliary cost for planning that penalizes collisions between the end-effector in its pre-push pose and the object for each push step in the plan. We note that no amount of training data can remedy this condition since even in simulation such an event is not possible, and it must instead be accounted for in the planning cost.

A second exploit occurs for no-op actions, i.e., valid skill executions that do not interact with the object and should then produce no change in the state of the object. Fig. 11c shows a push in which the end-effector starts in front of the object, and executes a push without ever touching the object. Because the training data did not contain such an instance, the model predicts it was an actual push and that the terminal state distribution will be located near the terminal pose of the end-effector after the push (orange meshes in Fig. 11c). We remedy this condition by augmenting the training data with no-op actions. Instead of collecting these instances in the simulator (which takes several hours), we take the nominal training set and generate synthetic no-op instances. For each initial object pose in the nominal set we generate random pushes and check for collisions between the end-effector and the object using Trimesh [22]. If any collision is detected, that sample is rejected, otherwise we set the initial and final object poses to be the initial object pose for the no-op sample. We collect $N = 5$ no-op samples per nominal instance and incorporate these into our training data. Fig. 11d shows the model prediction after the model is trained

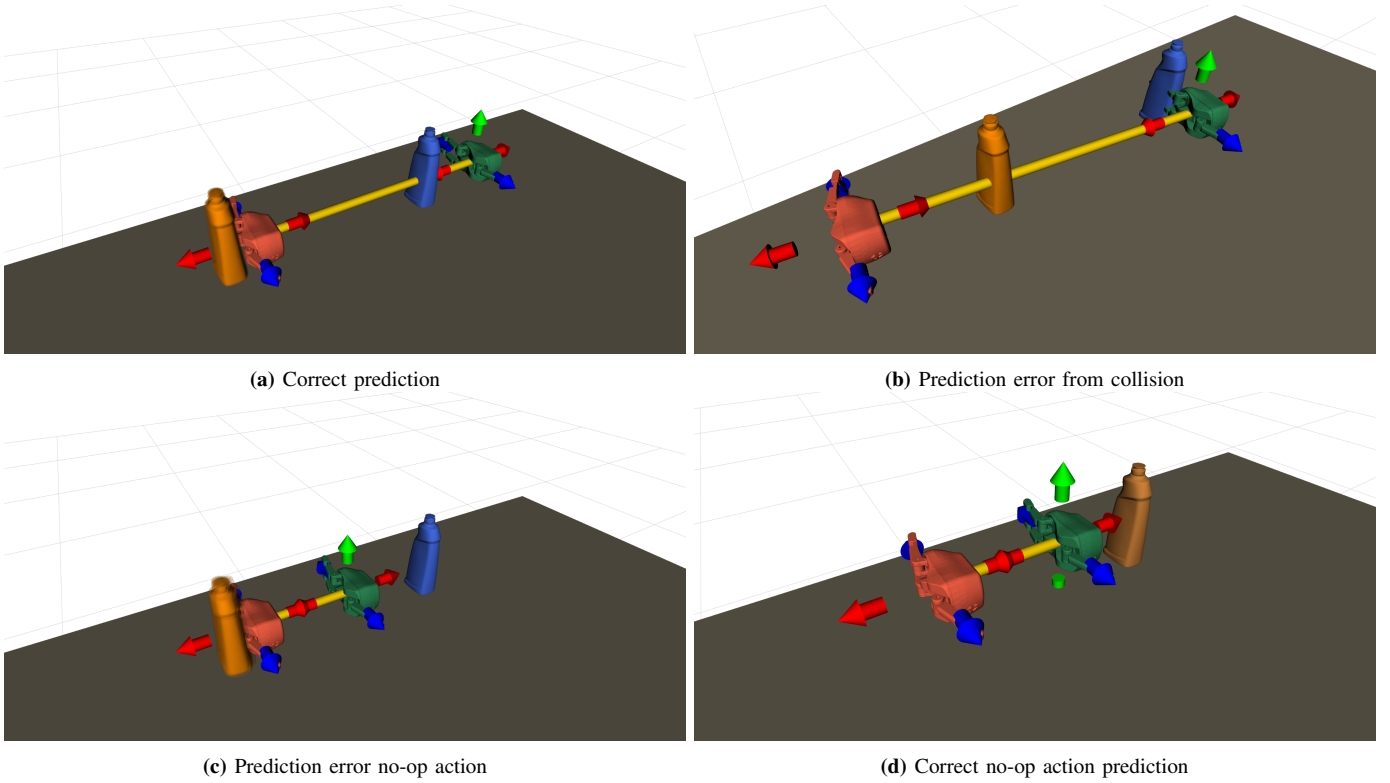


Fig. 11: Examples of the planner exploiting conditions outside the training data. Shown are initial object pose (blue mesh), predicted object pose distribution (orange meshes), start end-effector pose (green hand) and final end-effector pose (red mesh) for the push skill. **(a)** A correct outcome prediction for the push skill that we expect the planner to utilize. **(b)** The end-effector start pose is in a penetrating collision with the object, erroneously predicting it can relocate the object by executing a long push past the terminal object pose. **(c)** The end-effector begins in front-of the object, erroneously predicting a push. **(d)** A correct no-op prediction when the end-effector starts in front of the object after training data is augmented with no-op data.

with the augmented dataset. The model predicts the object distribution remains a tight Gaussian at the initial object pose, i.e., the action leaves the object undisturbed, as desired.